Chapter 8
Transition to Absolute Instability in Porous Media: Analytical Solutions

8.1 Absolute Instability in Porous Media

Most of the literature regarding the instability of flow in a porous medium is relative to the convective instability. The transition to absolute instability has been studied by some authors, but the literature on this specific subtopic is quite limited. One of the earlier papers on this subject is by Dufour and Néel [9].

The transition to absolute instability in the *Prats problem* is examined within an analytical and numerical study of the instability patterns of mixed convection in a horizontal porous channel. The Prats problem is a widely used denomination for the variant of the Horton–Rogers–Lapwood problem where the only changed feature is the presence of a forced horizontal flow. In fact, the original paper by Prats [12] develops the analysis of the onset of convective instability in a horizontal porous channel bounded by parallel impermeable and isothermal walls, with heating from below, and a uniform horizontal flow. Another study by Joulin and Ouarzazi [11] proposes a more complicated situation where the instability is not only driven by the heat transfer, which is induced by heating from below, but also by a simultaneous mass diffusion caused by the Soret effect. The latter physical effect consists in the existence of a solute mass flux contribution induced by the temperature gradient. Under these conditions, Joulin and Ouarzazi [11] present a thorough analysis of the transition from convective to absolute instability.

Delache et al. [7] further developed the investigation carried out by Dufour and Néel [9] on including also the form-drag term contribution in the momentum balance, i.e., by considering Darcy–Forchheimer's model instead of Darcy's law. These authors also suggest some interesting comparison with experimental results.

The analysis of the transition to absolute instability has been investigated also for non-Newtonian flows in porous media. This is the case of the studies presented by Hirata and Ouarzazi [10] and by Alves and Barletta [1]. The former study is relative to a viscoelastic fluid described through the Oldroyd-B model, while the latter deals with a power-law fluid.

A. Barletta, *Routes to Absolute Instability in Porous Media*,
https://doi.org/10.1007/978-3-030-06194-4_8

A wide research work has been carried out by Brevdo [6], Brevdo and Ruderman [4, 5], Diaz and Brevdo [8]. This work regarded cases where a vertical forced flow through a horizontal porous layer is accompanied by a prescribed horizontal temperature gradient. The authors concluded that the onset of convective instability coincides with the onset of absolute instability whenever the horizontal temperature gradient is zero. In fact, the effect of the horizontal temperature gradient is a secondary horizontal basic flow, which can induce the parametric delay in the onset of absolute instability with respect to convective instability.

The analysis of absolute instability in the Prats problem has been recently reconsidered by Barletta and Alves [2] and by Barletta and Celli [3]. In these papers, the effect of a finite Darcy–Prandtl number and that of an open upper boundary were considered, respectively. We mention that the Darcy–Prandtl number is a dimensionless parameter arising when convection problems in porous media are formulated starting from the local momentum balance given by Eq. (6.6), instead of the usual Darcy's law expressed by Eq. (6.5). When the Darcy–Prandtl number tends to infinity, the convection flow becomes compatible with the local momentum balance expressed by Eq. (6.5) [2].

8.2 Prats Problem

What is now well known as the Prats problem, after Prats [12], is the stability analysis of the uniform horizontal flow in a porous channel bounded by a pair of horizontal parallel planes, both impermeable and isothermal. A sketch of the horizontal porous layer is given in Fig. 8.1. We assume that the flow system is two-dimensional by considering all fields as independent of the spanwise y-coordinate. We also assume that the effect of viscous dissipation is negligible. When taken into account, this effect may alter significantly the stability analysis of the Prats problem.

The two-dimensional velocity field (u, w), lying in the (x, z) plane, the temperature field T, the coordinates (x, z) and time t, can be written in a dimensionless form by adopting the following transformations

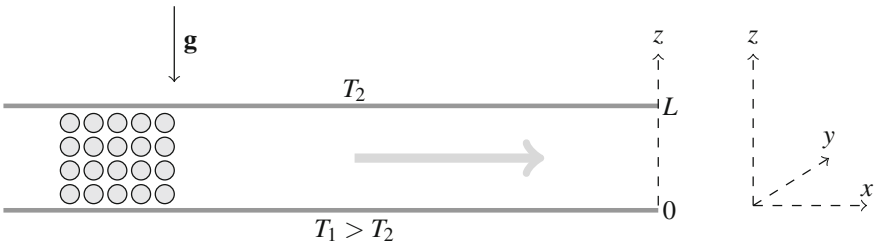

Fig. 8.1 A sketch of the horizontal porous channel, of the (x, y, z) coordinate frame and of the boundary conditions

$$(u, w)\,\frac{L}{\alpha} \to (u, w)\ , \qquad \frac{T - T_2}{T_1 - T_2} \to T\ ,$$
$$(x, z)\,\frac{1}{L} \to (x, z)\ , \qquad \frac{t}{L^2/\alpha} \to t\ . \tag{8.1}$$

Here, L is the height of the channel, as illustrated in Fig. 8.1, while α is the average thermal diffusivity of the porous medium.

Following the Oberbeck–Boussinesq approximation and Darcy's law, the local balance equations of mass, momentum and energy are written as

$$\frac{\partial u}{\partial x} + \frac{\partial w}{\partial z} = 0\ ,$$

$$\frac{\partial u}{\partial z} - \frac{\partial w}{\partial x} = -\,R\,\frac{\partial T}{\partial x}\ ,$$

$$\sigma\,\frac{\partial T}{\partial t} + u\,\frac{\partial T}{\partial x} + w\,\frac{\partial T}{\partial z} = \frac{\partial^2 T}{\partial x^2} + \frac{\partial^2 T}{\partial z^2}\ , \tag{8.2}$$

where σ is the ratio between the average volumetric heat capacity of the saturated porous medium and the volumetric heat capacity of the fluid. In Eq. (8.2), the local momentum balance has been formulated by evaluating the y component of the curl for Darcy's law. The Darcy–Rayleigh number R is defined as

$$R = \frac{g\beta(T_1 - T_2)KL}{\nu\alpha}\ , \tag{8.3}$$

where β is the thermal expansion coefficient of the fluid, and g is the modulus of the gravitational acceleration $\mathbf{g}$.

We prescribed the boundary conditions at $z = 0, 1$ as

$$z = 0\ :\quad w = 0\ ,\quad T = 1\ ,$$
$$z = 1\ :\quad w = 0\ ,\quad T = 0\ . \tag{8.4}$$

We introduce a streamfunction ψ, defined as

$$u = \frac{\partial \psi}{\partial z}\ , \qquad w = -\,\frac{\partial \psi}{\partial x}\ . \tag{8.5}$$

Thus, we satisfy the first equation (8.2), while the second and third differential equations (8.2) can be rewritten as

$$\frac{\partial^2 \psi}{\partial x^2} + \frac{\partial^2 \psi}{\partial z^2} + R\,\frac{\partial T}{\partial x} = 0\ ,$$

$$\sigma\,\frac{\partial T}{\partial t} + \frac{\partial \psi}{\partial z}\,\frac{\partial T}{\partial x} - \frac{\partial \psi}{\partial x}\,\frac{\partial T}{\partial z} = \frac{\partial^2 T}{\partial x^2} + \frac{\partial^2 T}{\partial z^2}\ . \tag{8.6}$$

The boundary conditions (8.4) are now expressed as

$$\begin{aligned} z = 0 \ : \quad & \frac{\partial \psi}{\partial x} = 0 \ , \quad T = 1 \ , \\ z = 1 \ : \quad & \frac{\partial \psi}{\partial x} = 0 \ , \quad T = 0 \ . \end{aligned} \tag{8.7}$$

8.2.1 The Basic Solution

There exists a stationary solution, $(\psi_\mathrm{b}, T_\mathrm{b})$, of Eqs. (8.6) and (8.7) describing a uniform velocity in the x-direction, and a pure conduction regime across the porous channel,

$$\psi_\mathrm{b} = Pe \ z \ , \qquad T_\mathrm{b} = 1 - z \ , \tag{8.8}$$

where

$$Pe = \frac{U_0 \, L}{\alpha} \tag{8.9}$$

is the *Péclet number* associated with the basic horizontal and uniform flow with constant velocity U_0 in the porous channel. One may easily check, from Eq. (8.5), that $\psi_\mathrm{b} = Pe \ z$ yields

$$u_\mathrm{b} = Pe \ , \qquad w_\mathrm{b} = 0 \ . \tag{8.10}$$

Without any loss of generality, we focus on the situation $Pe \geqslant 0$, as negative Péclet numbers do not identify physically different flow conditions.

8.2.2 Stability Analysis

Perturbations of the basic solution are defined as,

$$\psi = \psi_\mathrm{b} + \varepsilon \, \Psi \ , \qquad T = T_\mathrm{b} + \varepsilon \, \Theta \ , \tag{8.11}$$

where $|\varepsilon| \ll 1$. Let us substitute Eq. (8.11) into Eqs. (8.6) and (8.7), by taking into account Eq. (8.8) and by neglecting terms $O(\varepsilon^2)$. Thus, one obtains

$$\frac{\partial^2 \Psi}{\partial x^2} + \frac{\partial^2 \Psi}{\partial z^2} + R \, \frac{\partial \Theta}{\partial x} = 0 \ ,$$

$$\sigma \, \frac{\partial \Theta}{\partial t} + Pe \, \frac{\partial \Theta}{\partial x} + \frac{\partial \Psi}{\partial x} = \frac{\partial^2 \Theta}{\partial x^2} + \frac{\partial^2 \Theta}{\partial z^2} \ ,$$

$$z = 0, 1: \qquad \frac{\partial \Psi}{\partial x} = 0 \,, \quad \Theta = 0 \,. \tag{8.12}$$

We now express (Ψ, Θ) through their Fourier transforms,

$$\tilde{\Psi}(k, z, t) = \frac{1}{\sqrt{2\pi}} \int_{-\infty}^{\infty} e^{-\mathrm{i}\, k\, x}\, \Psi(x, z, t)\, \mathrm{d}\, x,$$

$$\Psi(x, z, t) = \frac{1}{\sqrt{2\pi}} \int_{-\infty}^{\infty} e^{\mathrm{i}\, k\, x}\, \tilde{\Psi}(k, z, t)\, \mathrm{d}\, k,$$

$$\tilde{\Theta}(k, z, t) = \frac{1}{\sqrt{2\pi}} \int_{-\infty}^{\infty} e^{-\mathrm{i}\, k\, x}\, \Theta(x, z, t)\, \mathrm{d}\, x \,,$$

$$\Theta(x, z, t) = \frac{1}{\sqrt{2\pi}} \int_{-\infty}^{\infty} e^{\mathrm{i}\, k\, x}\, \tilde{\Theta}(k, z, t)\, \mathrm{d}\, k \,, \tag{8.13}$$

and we also write

$$\tilde{\Psi} = f(z)\, \mathrm{e}^{\lambda(k)\, t} \,, \qquad \tilde{\Theta} = -\,\mathrm{i}\, k\, h(z)\, \mathrm{e}^{\lambda(k)\, t} \,. \tag{8.14}$$

Then, by employing Eqs. (8.13) and (8.14), we can apply the Fourier transform to Eq. (8.12) and obtain

$$\left(\frac{\mathrm{d}^2}{\mathrm{d}\, z^2} - k^2 \right) f + R\, k^2\, h = 0 \,,$$

$$\left[\frac{\mathrm{d}^2}{\mathrm{d}\, z^2} - k^2 - \sigma\, \lambda(k) - \mathrm{i}\, k\, Pe \right] h + f = 0 \,,$$

$$z = 0, 1 \ : \qquad f = 0 \,, \quad h = 0 \,. \tag{8.15}$$

The solution of the differential eigenvalue problem (8.15) is easily obtained by defining the parameter

$$\gamma(k) = \sigma\, \lambda(k) + \mathrm{i}\, k\, Pe \,, \tag{8.16}$$

so that Eq. (8.15) reads

$$\left(\frac{\mathrm{d}^2}{\mathrm{d}\, z^2} - k^2 \right) f + R\, k^2\, h = 0 \,,$$

$$\left[\frac{\mathrm{d}^2}{\mathrm{d}z^2} - k^2 - \gamma(k)\right] h + f = 0 \,,$$

$$z = 0, 1 \;: \qquad f = 0 \,, \quad h = 0 \,. \tag{8.17}$$

We can easily reckon that the eigenvalue problem (8.17) coincides with that formulated for the Horton–Rogers–Lapwood problem, expressed by Eqs. (7.75) and (7.76). The only difference is that, in Eq. (8.17), γ appears instead of λ. The obvious consequence is that the analytical dispersion relation written for Eq. (8.17) is easily retrieved from Eq. (7.79), namely

$$(n^2\pi^2 + k^2)\left[\gamma(k) + n^2\pi^2 + k^2\right] - Rk^2 = 0 \,, \quad n = 1, 2, 3, \ldots \,. \tag{8.18}$$

One can solve Eq. (8.18) for $\gamma(k)$ and obtain

$$\gamma(k) = \frac{Rk^2 - (n^2\pi^2 + k^2)^2}{n^2\pi^2 + k^2} \,, \quad n = 1, 2, 3, \ldots \,. \tag{8.19}$$

8.2.3 *Convective Instability*

Equation (8.19) is the starting point for both the study of convective instability and that of absolute instability. As for the convective instability, we have to take $k \in \mathbb{R}$ and separate the real and the imaginary parts of Eq. (8.19). We must remember that $\lambda = \eta - \mathrm{i}\,\omega$, where η is the growth rate of the normal mode and ω is the angular frequency. Then, on account of Eqs. (8.16) and (8.19), we can write

$$\eta = \frac{Rk^2 - (n^2\pi^2 + k^2)^2}{\sigma\left(n^2\pi^2 + k^2\right)} \,, \quad \omega = \frac{k\,Pe}{\sigma} \,, \quad n = 1, 2, 3, \ldots \,. \tag{8.20}$$

The first conclusion which can be drawn from Eq. (8.20) regards the angular frequency. The meaning of the equation $\omega = k\,Pe/\sigma$ is that the dimensionless phase velocity of the normal mode with wave number k is a constant, $\omega/k = Pe/\sigma$. The physical implications of this finding are that the normal modes travel along the x-direction with a dimensionless phase velocity different from the dimensionless velocity of the basic flow, Pe. The former can be greater, equal or smaller than the latter depending on the heat capacity ratio, σ, being smaller, equal or greater than 1, respectively. This conclusion can be correctly established only with length, time and velocity scales defined consistently, as we did in Eq. (8.1). The consistency means, in particular, that the velocity scale is the ratio of the length scale and the timescale. Such consistent choice of the scales in defining the dimensionless quantities is an unnecessary complication when handling the Horton–Rogers–Lapwood problem, or its variants explored in Chap. 7. In fact, in those cases, the principle of exchange of stabilities ensures that the phase velocity of the disturbances involved in the onset

of convective instability is zero. Incidentally, the principle of exchange of stabilities is implied by the equation $\omega/k = Pe/\sigma$, as one may easily recognise that the Horton–Rogers–Lapwood problem is nothing but the limiting case of the Prats problem when $Pe \to 0$.

The second conclusion drawn from Eq. (8.20) regards the threshold for the onset of convective instability. Indeed, convective instability arises when the growth rate η becomes positive, i.e. when

$$R > \frac{(\pi^2 + k^2)^2}{k^2} \,, \tag{8.21}$$

while the neutral stability condition is

$$R = \frac{(\pi^2 + k^2)^2}{k^2} \,. \tag{8.22}$$

Both Eqs. (8.21) and (8.22) have been obtained by considering the modes with $n = 1$ as these modes yield the lowest threshold values of R for attaining positive growth rates, $\eta > 0$. The neutral stability function $R(k)$ defined by Eq. (8.22) just coincides with that obtained for the Horton–Rogers–Lapwood problem and given by Eq. (7.82). Obviously, the critical values of k and R are still given by Eq. (7.83).

We remark that the neutral stability condition (8.22) is not influenced by the Péclet number, Pe. The only effect of the horizontal flow regards the travelling nature of the normal modes. The phase velocity tends to zero in the limit $Pe \to 0$, when the Prats problem coincides with the Horton–Rogers–Lapwood problem. Thus, in this limit, one recovers the principle of exchange of stabilities.

8.2.4 *Absolute Instability*

In the analysis of absolute instability, one has to test the asymptotic behaviour of the wave packets,

$$\Psi(x, z, t) = \frac{1}{\sqrt{2\pi}} \int_{-\infty}^{\infty} \mathrm{e}^{\lambda(k)\, t + \mathrm{i}\, k\, x} f(z)\, \mathrm{d}\, k \,,$$

$$\Theta(x, z, t) = -\frac{\mathrm{i}}{\sqrt{2\pi}} \int_{-\infty}^{\infty} k\, \mathrm{e}^{\lambda(k)\, t + \mathrm{i}\, k\, x} h(z)\, \mathrm{d}\, k \,, \tag{8.23}$$

when $t \to \infty$. Equation (8.23) is obtained by substituting Eq. (8.14) into Eq. (8.13). We point out that $f(z)$ and $h(z)$, being determined by solving Eq. (8.15), do depend on k in general. Detecting the asymptotic behaviour at large time of the wave packets given by Eq. (8.23) means adopting the steepest-descent approximation. This approximation is illustrated in Sect. 3.5.3. Simple applications of this

method to the analysis of absolute instability have been discussed in Chap. 4. In fact, absolute instability means that

$$\lim_{t\to+\infty} |\Psi(x,z,t)| = \infty \,, \qquad \lim_{t\to+\infty} |\Theta(x,z,t)| = \infty \,, \tag{8.24}$$

for every $x \in \mathbb{R}$, with $0 < z < 1$. We mention that the wave packets given by Eq. (8.23) implicitly depend on $n = 1, 2, 3, \ldots$. Then, one should define general wave packet perturbations by summing up Fourier integrals with different n. This aspect can be safely left implicit provided that one tests compliance of the limiting conditions (8.24) for, at least, one value of n.

The method based on the steepest-descent approximation is very powerful as it reveals that the fulfilment of the limiting conditions (8.24) just depends on the properties of the dispersion relation (8.19). In fact, from Eq. (8.16), Eq. (8.19) can be rewritten as

$$\sigma\,\lambda(k) = \frac{R\,k^2 - (n^2\pi^2 + k^2)^2}{n^2\pi^2 + k^2} - \mathrm{i}\,k\,Pe \,, \quad n = 1, 2, 3, \ldots \,. \tag{8.25}$$

As illustrated in Sect. 4.2.1, the first step is determining the saddle points of $\lambda(k)$. In other words, we have to determine the roots of equation

$$\lambda'(k) = 0 \,, \tag{8.26}$$

in the complex plane, $k \in \mathbb{C}$. Equations (8.25) and (8.26) yield

$$\frac{2\,k\,R\,n^2\pi^2}{(n^2\pi^2 + k^2)^2} = 2\,k + \mathrm{i}\,Pe \,. \tag{8.27}$$

The solution of Eq. (8.27) is particularly simple in the limiting case of no horizontal flow, $Pe = 0$, namely for the Horton–Rogers–Lapwood problem. In this special case, Eq. (8.27) yields four saddle points, given by

$$k_0^2 = -\,n^2\pi^2 \pm R^{1/2}\,n\,\pi \,. \tag{8.28}$$

With the minus sign in Eq. (8.28), we obtain two purely imaginary saddle points,

$$k_0 = \mathrm{i}\,\sqrt{n^2\pi^2 + R^{1/2}\,n\,\pi} \,, \qquad k_0 = -\,\mathrm{i}\,\sqrt{n^2\pi^2 + R^{1/2}\,n\,\pi} \,. \tag{8.29}$$

Equation (8.25) implies that $\lambda(k)$ has two singularities given by the imaginary simple poles

$$k = \mathrm{i}\,n\,\pi \,, \qquad k = -\mathrm{i}\,n\,\pi \,. \tag{8.30}$$

Then, we conclude that it is impossible to deform continuously the real line $\Im(k) = 0$, without sweeping the two singularities given by Eq. (8.30), so that it becomes locally

a line of steepest descent through the saddle points given by Eq. (8.29). In other words, the two saddle points expressed by Eq. (8.29) are not involved in the steepest-descent approximation of the wave packets defined by Eq. (8.23). Then, we must exclude these saddle points in evaluating the threshold value of R for absolute instability. We are left with the two saddle points given by

$$k_0^2 = -n^2\pi^2 + R^{1/2}\, n\,\pi \ . \tag{8.31}$$

When Eq. (8.31) is substituted into Eq. (8.25) with $Pe = 0$, one has

$$\sigma\ \lambda(k_0) = R^{1/2}\ \left(R^{1/2} - 2\,n\,\pi\right) \ . \tag{8.32}$$

Equation (8.32) reveals that $\lambda(k_0)$ is real and that it is positive when

$$R > 4\,n^2\pi^2 \ . \tag{8.33}$$

This inequality establishes the condition for the onset of absolute instability. In fact, the threshold value $R = R_\mathrm{a}$ for absolute instability is obtained from Eq. (8.33) by considering the most unstable case, namely $n = 1$. Thus, we can write

$$R_\mathrm{a} = 4\,\pi^2 \ . \tag{8.34}$$

By comparing Eqs. (7.83) and (8.34), one can conclude that the threshold value of R for the onset of absolute instability, R_a, coincides with the critical value, R_c. In other words, when instability arises with $Pe = 0$, it is both convective and absolute. This conclusion is what one should expect on purely physical grounds. In fact, we pointed out in Sect. 4.2.1 that absolute instability differs from convective instability inasmuch as there exists a flow which drives the perturbation modes downstream. Such flow can be so intense as to conceal the actual time growth of some normal modes included in a perturbation wave packet by convecting away such modes. When the basic flow is switched off, that is when $Pe = 0$, convective instability implies absolute instability, so that the two thresholds R_c and R_a coincide.

By employing the threshold value of R given by Eq. (8.34), we can evaluate the pertinent saddle points through Eq. (8.31). We obtain

$$k_0 = \pm\,\pi \ . \tag{8.35}$$

On account of Eq. (7.83), this means that the two saddle points lie on the real axis and that $k_0 = \pm\, k_\mathrm{c}$.

Another sensible comment regards the role played by parameter σ. We said that σ does not influence the parametric threshold for convective stability, expressed by Eq. (8.22). We can also infer that the threshold for absolute instability is not influenced by the value of σ, as well. From Eq. (8.34), this is quite evident in the case $Pe = 0$. When $Pe > 0$, just the same conclusion is expected as the saddle points k_0 are evaluated by solving Eq. (8.27) which does not contain σ. Moreover, the condition

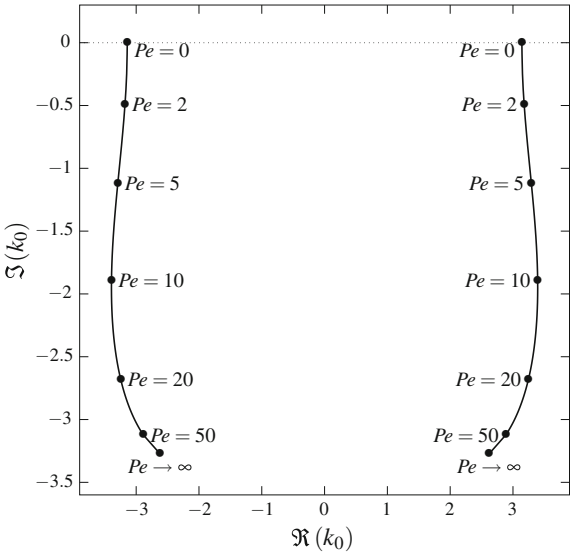

Fig. 8.2 Prats problem: migration of the pertinent saddle points, with increasing values of Pe, for the threshold to absolute instability

of absolute instability is determined by the inequality $\Re(\lambda(k_0)) > 0$, or equivalently $\sigma\,\Re(\lambda(k_0)) > 0$, by employing Eq. (8.25). The right-hand side of Eq. (8.25) does not contain σ. Thus, we conclude that the value of σ only affects the phase velocity of the normal mode perturbations driving the instability.

When $Pe > 0$, detecting the saddle points by employing Eqs. (8.25) and (8.27) implies the solution of a system of two algebraic equations, that is $\lambda'(k_0) = 0$ and $\Re(\lambda(k_0)) = 0$. This means that we find multiple complex roots of Eq. (8.27) for every value of $Pe > 0$. Each saddle point k_0 is associated with a uniquely determined real value of R. By analogy with what we found for the case $Pe = 0$, we expect that just two of these roots represent the pertinent saddle points for establishing the value of R_a. The value of R_a is to be obtained from Eq. (8.25) through the condition $\Re(\lambda(k_0)) = 0$, which yields the threshold for absolute instability.

The practical strategy is starting from $Pe = 0$ and gradually increasing Pe. We assume $n = 1$, consistently with what we did for the case $Pe = 0$. Step by step, one tracks the migration of the saddle points k_0 starting from those found with $Pe = 0$, and given by Eq. (8.35). With each of these saddle points, one evaluates the associated value of R as the root of $\Re(\lambda(k_0)) = 0$. The position of the saddle points which are relevant for the onset of absolute instability is illustrated in Fig. 8.2. Such points are tracked for increasing values of $Pe > 0$. For each value of Pe, there are two twin points differing only by the sign of the real part of k_0. They originate from the pair defined by Eq. (8.35), with $Pe = 0$, and they have drifted to negative values of $\Im(k_0)$, when $Pe > 0$.

There are multiple saddle points k_0 for every assignment of (n, Pe, R). One then associates a value of R to every fixed pair (n, Pe), by imposing the third algebraic equation $\Re(\lambda(k_0)) = 0$. Such procedure can be practically illustrated by considering the case where $n = 1$ and $Pe = 10$. We obtain

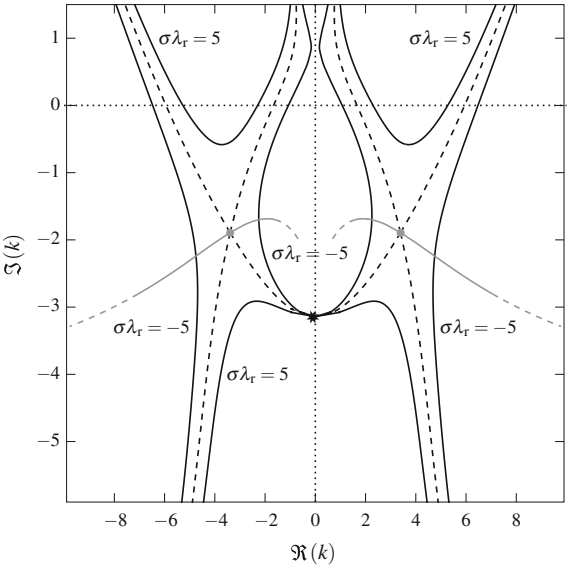

Fig. 8.3 Prats problem: map of the isolines of $\Re(\lambda) = \lambda_r$ (black solid lines) for $Pe = 10$ and $R = R_a = 57.8036$. The dashed black lines are for $\lambda_r = 0$. The grey dots are the saddle points, while the grey lines are the lines of steepest descent. The black asterisk denotes the singularity $k = -i\pi$

$$k_0 = \pm 3.39297 - i\,1.89300\,, \qquad R = 57.8036\,,$$

$$k_0 = \pm 1.84692 + i\,3.39151\,, \qquad R = -36.0935\,,$$

$$k_0 = i\,1.51492\,, \qquad R = 25\,,$$

$$k_0 = -i\,6.51492\,, \qquad R = 25\,. \tag{8.36}$$

We have to exclude the saddle points $k_0 = \pm 1.84692 + i\,3.39151$ as they would yield a negative value of R for the onset of absolute instability, -36.0935, which is unphysical given that we must get $R_a \geqslant R_c$. Just the same argument leads us to the exclusion of the purely imaginary saddle points $k_0 = i\,1.51492$ and $k_0 = -i\,6.51492$. This means that, with $Pe = 10$, the pertinent saddle points for the onset of absolute instability are $k_0 = \pm 3.39297 - i\,1.89300$ and that the threshold for the onset of absolute instability is $R_a = 57.8036$. All this reasoning is to be completed by checking whether the holomorphy requirement is satisfied with $Pe = 10$, $R_a = 57.8036$ and the pair of saddle points $k_0 = \pm 3.39297 - i\,1.89300$.

Figure 8.3 displays a map of the isolines of $\Re(\lambda) = \lambda_r$ in the complex k plane relative to the case $Pe = 10$ and $R = R_a = 57.8036$. The lines of steepest descent crossing the twin saddle points $k_0 = \pm 3.39297 - i\,1.89300$ are displayed in grey. It is evident from Fig. 8.3 that one can continuously deform the path γ given by the real axis, $\Im(k) = 0$, into a path γ^* which crosses both the twin saddle points, $k_0 = \pm 3.39297 - i\,1.89300$. Such deformation can be exploited so that γ^* locally coincides with a line of steepest descent and no singularity of $\lambda(k)$ is enclosed within the region bounded by $\gamma \cup \gamma^*$, as described in Sect. 3.5.3. Then, the premises

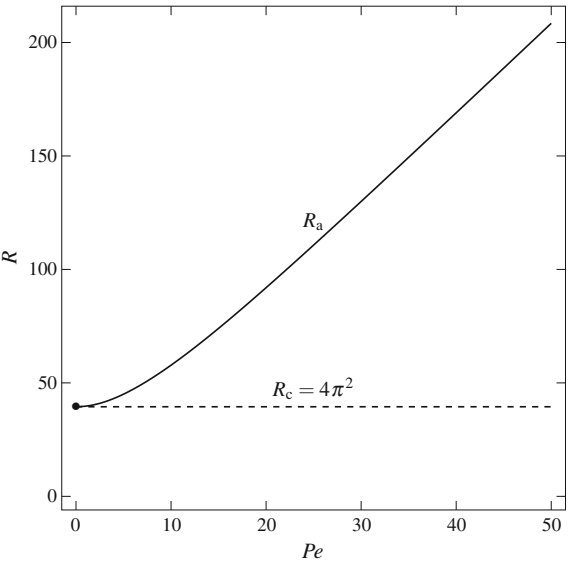

Fig. 8.4 Prats problem: plot of R_a versus Pe as obtained by solving Eq. (8.27) with $\Re(\lambda(k)) = 0$. The values of R_a are compared with $R_c = 4\pi^2$, which is independent of Pe

for applying the steepest-descent approximation, denoted under the shorthand of holomorphy requirement, are all satisfied.

One may wonder whether taking $n > 1$ can affect the conclusion just drawn for $Pe = 10$. If one sets $n = 2$, Eq. (8.36) is to be replaced with

$$\begin{aligned} k_0 &= \pm 6.58511 - \mathrm{i}\, 2.24028 \,, \qquad R = 180.111 \,, \\ k_0 &= \pm 3.02861 + \mathrm{i}\, 6.72099 \,, \qquad R = -69.4442 \,, \\ k_0 &= \mathrm{i}\, 4.26228 \,, \qquad R = 25 \,, \\ k_0 &= -\mathrm{i}\, 9.26228 \,, \qquad R = 25 \,. \end{aligned} \tag{8.37}$$

Again, the values $R = -69.4442$ and $R = 25$ are to be excluded as possible candidates for R_a as they are smaller than R_c. Then, one is left with $R = 180.111$ that, in any case, does not provide a lower threshold to absolute instability than that obtained by considering $n = 1$.

This lengthy description refers to the evaluation of R_a for a very special case, that is, $Pe = 10$. It should be ideally repeated for every value of Pe. In practice, such a check of the holomorphy requirement can only be carried out for a finite number of values of Pe. What one concludes is that the evaluation of R_a can be practically achieved, for a given Pe, by tracking the continuous change of the twin saddle points given by Eq. (8.35) for $Pe = 0$. The resulting evaluation of R_a versus Pe is illustrated in Fig. 8.4. This figure shows that, starting with $R_a = R_c = 4\pi^2$ for $Pe = 0$, a gap exists between the thresholds of convective and absolute instabilities as Pe increases above zero. This gap grows larger and larger with Pe.

A feature highlighted by Fig. 8.4 is the linear behaviour in the trend of R_a versus Pe when Pe becomes very large. The characteristics of this asymptotic regime can be detected by setting

$$R = \xi \, Pe \, , \tag{8.38}$$

where ξ is a constant to be determined. We substitute Eq. (8.38) into Eq. (8.27), and we let $Pe \to \infty$. What we obtain is

$$\frac{2 \, k \, \xi \, n^2 \pi^2}{(n^2 \pi^2 + k^2)^2} = \mathrm{i} \, , \tag{8.39}$$

while the dispersion relation (8.25) can be approximated as

$$\frac{\sigma \, \lambda(k)}{Pe} = \frac{\xi \, k^2}{n^2 \pi^2 + k^2} - \mathrm{i} \, k \, , \quad n = 1, 2, 3, \ldots \, . \tag{8.40}$$

The saddle points k_0 and the corresponding values of ξ are obtained by solving the system made with equations (8.39) and $\Re(\sigma \, \lambda(k)/Pe) = 0$, as expressed by employing Eq. (8.40). The result is

$$\begin{aligned} k_0 &= \pm \frac{\pi \, n}{4} \sqrt{7 + \sqrt{17}} - \frac{\mathrm{i} \, \pi \, n}{4} \sqrt{5 + 3\sqrt{17}} \, , \quad \xi = \frac{\pi \, n}{8} \sqrt{51 \sqrt{17} - 107} \, , \\ k_0 &= \pm \frac{\pi \, n}{4} \sqrt{7 + \sqrt{17}} + \frac{\mathrm{i} \, \pi \, n}{4} \sqrt{5 + 3\sqrt{17}} \, , \quad \xi = -\frac{\pi \, n}{8} \sqrt{51 \sqrt{17} - 107} \, . \end{aligned} \tag{8.41}$$

Obviously, the saddle points leading to a negative ξ are to be rejected as $R_a = \xi \, Pe$, with $Pe > 0$, cannot be negative. Thus, the pair of twin saddle points leading to the threshold of absolute instability in the limit $Pe \to \infty$ is

$$k_0 = \pm \frac{\pi \, n}{4} \sqrt{7 + \sqrt{17}} - \frac{\mathrm{i} \, \pi \, n}{4} \sqrt{5 + 3\sqrt{17}} \approx (\pm 2.61941 - \mathrm{i} \, 3.27327) \, n \, . \tag{8.42}$$

For $n = 1$, the pair of saddle points given by Eq. (8.42) are displayed in Fig. 8.2. One may easily reckon that the location of the saddle points pertinent for evaluating the threshold to absolute instability tends to attain rapidly its asymptotic settlement, defined by Eq. (8.42) with $n = 1$, when Pe becomes larger than 50.

The attainment of the asymptotic regime is in fact illustrated in Fig. 8.5, where the trend of R_a/Pe versus Pe is displayed. This figure shows the asymptote,

$$\frac{R_a}{Pe} = \frac{\pi}{8} \sqrt{51 \sqrt{17} - 107} \approx 3.99084 \, , \tag{8.43}$$

as a dotted line. One may evaluate that R_a/Pe matches its asymptotic value within less than 5 % when $Pe > 45.5$.

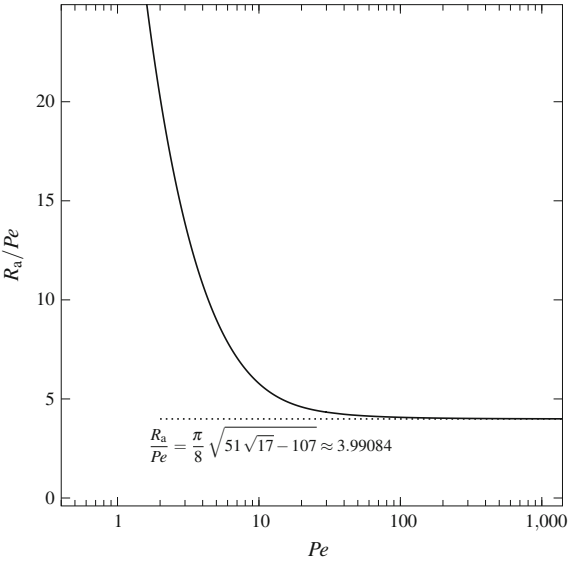

Fig. 8.5 Prats problem: plot of R_a/Pe versus Pe as compared with the asymptotic behaviour for large values of Pe (dotted line) given by Eq. (8.43)

Table 8.1 reports the threshold data defining the transition to absolute instability. The whole range of positive Péclet numbers is spanned, thus showing the extrema of very small Pe, where R_a approaches $R_c = 4\pi^2$, and that of very large Pe, where R_a/Pe approaches its asymptotic value given by Eq. (8.43).

Regarding the possible saddle points obtained by solving Eq. (8.27), for a given (Pe, n), a comment is desirable regarding those expressed analytically as

$$k_0 = -\frac{i}{4}\left(Pe \pm \sqrt{16\,n^2\pi^2 + Pe^2}\right) . \tag{8.44}$$

These saddle points yield simultaneously $\Re(\lambda(k_0)) = 0$ and $\Im(\lambda(k_0)) = 0$, with

$$R = \frac{Pe^2}{4} . \tag{8.45}$$

This family of solutions of the dispersion relation (8.27) has been encountered either in Eq. (8.36) or in Eq. (8.37) relative to the sample case $Pe = 10$ with $n = 1$ and $n = 2$, respectively. In that example, we excluded these saddle points as they were subcritical with $R = Pe^2/4 = 25 < R_c$. However, this is not always the case. In fact, for $n = 1$, these solutions regard the supercritical domain for $Pe > 4\pi \approx 12.5664$ and, provided that Pe is less than approximately 18.6583, they are associated with values of $R = Pe^2/4$ smaller than the values of R_a evaluated so far and reported either in Fig. 8.4 or in Table 8.1. Does it mean that we should amend our conclusions about the threshold to absolute instability for the range $4\pi < Pe < 18.6583$? The answer is negative. If these saddle points were to contribute to the evaluation of R_a, then k_0 should coincide with $k_c = \pi$ when $Pe = 4\pi$ and $R_a = R_c$, but this is

Table 8.1 Prats problem: pertinent saddle points and threshold values of R_a for the onset of absolute instability

Pe	k_0	R_a	R_a/Pe
0	± 3.14159	39.4784	∞
1	$\pm 3.15128 - \mathrm{i}\,0.24846$	39.7269	39.7269
5	$\pm 3.29255 - \mathrm{i}\,1.12014$	45.0277	9.00553
7	$\pm 3.35371 - \mathrm{i}\,1.46714$	49.5519	7.07884
10	$\pm 3.39297 - \mathrm{i}\,1.89300$	57.8036	5.78036
15	$\pm 3.34682 - \mathrm{i}\,2.38924$	74.0236	4.93491
20	$\pm 3.24476 - \mathrm{i}\,2.68308$	91.9528	4.59764
25	$\pm 3.14596 - \mathrm{i}\,2.85317$	110.732	4.42926
30	$\pm 3.06606 - \mathrm{i}\,2.95566$	129.947	4.33158
35	$\pm 3.00401 - \mathrm{i}\,3.02135$	149.404	4.26868
40	$\pm 2.95570 - \mathrm{i}\,3.06602$	169.003	4.22506
45	$\pm 2.91750 - \mathrm{i}\,3.09797$	188.692	4.19315
50	$\pm 2.88675 - \mathrm{i}\,3.12176$	208.441	4.16882
60	$\pm 2.84058 - \mathrm{i}\,3.15458$	248.054	4.13424
70	$\pm 2.80776 - \mathrm{i}\,3.17599$	287.761	4.11087
80	$\pm 2.78332 - \mathrm{i}\,3.19097$	327.522	4.09403
90	$\pm 2.76444 - \mathrm{i}\,3.20201$	367.319	4.08133
100	$\pm 2.74943 - \mathrm{i}\,3.21048$	407.140	4.07140
1000	$\pm 2.63194 - \mathrm{i}\,3.26797$	3998.25	3.99825
∞	$\pm 2.61941 - \mathrm{i}\,3.27327$	∞	3.99084

obviously not the case. Another reason is the following. For every Pe within the range $4\pi < Pe < 18.6583$ and for $n = 1$, the two saddle points given by Eq. (8.44) and corresponding to $Ra = Pe^2/4$ are purely imaginary. One lies between the two singularities $k = \pm \mathrm{i}\,\pi$, while the other one lies below $k = -\mathrm{i}\,\pi$. Trying to draw a deformed path, which is locally of steepest descent and which crosses both these saddle points is not possible without trapping the singularity $k = -\mathrm{i}\,\pi$ within the region of space between the deformed path and the real k-axis. This feature precludes the application of the holomorphy requirement. Thus, we infer that the branches of saddle points defined by Eq. (8.44) are not genuine branches of absolute instability, so that they can be disregarded.

8.3 Prats Problem with Form-Drag Effect

We now explore how our analysis of convective and absolute instabilities in the Prats problem changes by assuming Darcy–Forchheimer's law, instead of Darcy's law, to model the local momentum balance. Again, we carry out a two-dimensional study by assuming that all fields are independent of the spanwise y-coordinate. As in Sect. 8.2, we neglect the effect of viscous dissipation for the sake of simplicity.

The two-dimensional velocity field (u, w), lying in the (x, z) plane, the temperature field T, the coordinates (x, z) and time t, can be written in a dimensionless form by adopting the transformation (8.1).

Following Eq. (7.84), within the Oberbeck–Boussinesq approximation and according to Darcy–Forchheimer's law, the local balance equations of mass, momentum and energy are given by

$$\frac{\partial u}{\partial x} + \frac{\partial w}{\partial z} = 0 \,,$$

$$\frac{\partial(\Xi\, u)}{\partial z} - \frac{\partial(\Xi\, w)}{\partial x} = -\, R\, \frac{\partial T}{\partial x} \,,$$

$$\sigma\, \frac{\partial T}{\partial t} + u\, \frac{\partial T}{\partial x} + w\, \frac{\partial T}{\partial z} = \frac{\partial^2 T}{\partial x^2} + \frac{\partial^2 T}{\partial z^2} \,. \tag{8.46}$$

In Eq. (8.46), the local momentum balance has been formulated by evaluating the curl of the local momentum balance. Function Ξ is defined as

$$\Xi = 1 + G\, \sqrt{u^2 + w^2} \,, \tag{8.47}$$

while the dimensionless parameters R and G are given by

$$R = \frac{g\beta(T_1 - T_2)KL}{\nu\alpha} \,, \qquad G = \frac{F\alpha\sqrt{K}}{\nu L} \,, \tag{8.48}$$

where F is the form-drag coefficient. The governing equations (8.46) are completed by the boundary conditions,

$$\begin{aligned} z = 0 \;:&\quad w = 0 \,, \quad T = 1 \,, \\ z = 1 \;:&\quad w = 0 \,, \quad T = 0 \,. \end{aligned} \tag{8.49}$$

By analogy with Eq. (8.6), we write a streamfunction–temperature formulation of the governing equations and boundary conditions

$$\frac{\partial}{\partial x}\left(\Xi\, \frac{\partial \psi}{\partial x}\right) + \frac{\partial}{\partial z}\left(\Xi\, \frac{\partial \psi}{\partial z}\right) + R\, \frac{\partial T}{\partial x} = 0 \,,$$

$$\sigma\, \frac{\partial T}{\partial t} + \frac{\partial \psi}{\partial z}\, \frac{\partial T}{\partial x} - \frac{\partial \psi}{\partial x}\, \frac{\partial T}{\partial z} = \frac{\partial^2 T}{\partial x^2} + \frac{\partial^2 T}{\partial z^2} \,,$$

$$\begin{aligned} z = 0 \;:&\quad \frac{\partial \psi}{\partial x} = 0 \,, \quad T = 1 \,, \\ z = 1 \;:&\quad \frac{\partial \psi}{\partial x} = 0 \,, \quad T = 0 \,. \end{aligned} \tag{8.50}$$

The same stationary solution, (ψ_b, T_b), expressed by Eqs. (8.8) and (8.9) satisfies also Eq. (8.50). We already pointed out that this solution describes a uniform flow, in the x-direction, with a dimensionless rate expressed by the Péclet number Pe and with a linear temperature distribution along the vertical z-direction. We implicitly consider $Pe \geqslant 0$, as a sign change of Pe does not correspond to physically different situations.

8.3.1 Stability Analysis

We assume perturbations of the basic solution given by,

$$\psi = \psi_b + \varepsilon\, \Psi = Pe\, z + \varepsilon\, \Psi\ , \qquad T = T_b + \varepsilon\, \Theta = 1 - z + \varepsilon\, \Theta\ , \tag{8.51}$$

where $|\varepsilon| \ll 1$. On substituting Eq. (8.51) into Eq. (8.50) and neglecting terms $O(\varepsilon^2)$, one obtains

$$\begin{gathered}
(1 + G\ Pe)\, \frac{\partial^2 \Psi}{\partial x^2} + (1 + 2\, G\ Pe)\, \frac{\partial^2 \Psi}{\partial z^2} + R\, \frac{\partial \Theta}{\partial x} = 0\ , \\
\sigma\ \frac{\partial \Theta}{\partial t} + Pe\ \frac{\partial \Theta}{\partial x} + \frac{\partial \Psi}{\partial x} = \frac{\partial^2 \Theta}{\partial x^2} + \frac{\partial^2 \Theta}{\partial z^2}\ , \\
z = 0, 1\ : \qquad \frac{\partial \Psi}{\partial x} = 0\ , \quad \Theta = 0\ .
\end{gathered} \tag{8.52}$$

Following the usual procedure, established with Eq. (8.13), we write (Ψ, Θ) in terms of their Fourier transforms, $\left(\tilde{\Psi}, \tilde{\Theta}\right)$, given by

$$\tilde{\Psi} = f(z)\, \mathrm{e}^{\lambda(k)\, t}\ , \qquad \tilde{\Theta} = -\,\mathrm{i}\, k\, h(z)\, \mathrm{e}^{\lambda(k)\, t}\ . \tag{8.53}$$

Then, by employing Eqs. (8.13) and (8.53), we employ the Fourier transformation for Eq. (8.52) to write

$$\begin{gathered}
\left[(1 + 2\, G\ Pe)\, \frac{\mathrm{d}^2}{\mathrm{d}\, z^2} - (1 + G\ Pe)\, k^2\right] f + R\, k^2\, h = 0\ , \\
\left[\frac{\mathrm{d}^2}{\mathrm{d}\, z^2} - k^2 - \sigma\, \lambda(k) - \mathrm{i}\, k\, Pe\right] h + f = 0\ , \\
z = 0, 1\ : \qquad f = 0\ , \quad h = 0\ .
\end{gathered} \tag{8.54}$$

The eigenvalue problem (8.54) is solved by combining the two ordinary differential equations into a single one,

$$\left[(1+2\,G\,Pe)\,\frac{\mathrm{d}^2}{\mathrm{d}\,z^2}-(1+G\,Pe)\,k^2\right]\left[\frac{\mathrm{d}^2}{\mathrm{d}\,z^2}-k^2-\gamma(k)\right]h-R\,k^2\,h=0\;, \tag{8.55}$$

where $\gamma(k)$ is defined in the same manner as in the analysis of the Prats problem carried out in terms of Darcy's law, namely

$$\gamma(k)=\sigma\,\lambda(k)+\mathrm{i}\,k\,Pe\;. \tag{8.56}$$

The eigenfunction $h(z)$ can be expressed as

$$h(z)=\sin(n\,\pi\,z)\;,\quad n=1,2,3,\;\ldots\;, \tag{8.57}$$

so that the boundary conditions (8.54) are satisfied, while substitution of Eq. (8.57) into Eq. (8.55) yields the dispersion relation

$$\left[(1+2\,G\,Pe)\,n^2\,\pi^2+(1+G\,Pe)\,k^2\right]\left[n^2\,\pi^2+k^2+\gamma(k)\right]-R\,k^2=0\;. \tag{8.58}$$

Equation (8.58) can be solved for $\gamma(k)$ to obtain

$$\gamma(k)=\frac{R\,k^2-\left[(1+2\,G\,Pe)\,n^2\,\pi^2+(1+G\,Pe)\,k^2\right]\left(n^2\,\pi^2+k^2\right)}{(1+2\,G\,Pe)\,n^2\,\pi^2+(1+G\,Pe)\,k^2}\;, \tag{8.59}$$

with $n=1,2,3,\;\ldots$.

8.3.2 *Convective Instability*

The analysis of the convective instability for the Prats problem with form-drag effect has been carried out by Rees [13].

By recalling that $\lambda=\eta-\mathrm{i}\,\omega$ and by taking into account Eq. (8.56), the imaginary part of the dispersion relation (8.58) yields

$$(\sigma\,\omega-k\,Pe)\left[(1+2\,G\,Pe)\,n^2\,\pi^2+(1+G\,Pe)\,k^2\right]=0\;. \tag{8.60}$$

Thus, we obtain just the same expression of ω as given by Eq. (8.20) for the case where the validity of Darcy's law is invoked,

$$\omega=\frac{k\,Pe}{\sigma}\;. \tag{8.61}$$

As a consequence, we reach the same conclusion discussed for the case of Darcy's flow. The phase velocity of the normal mode with wave number k is a constant, $\omega/k = Pe/\sigma$. On the other hand, the expression of the growth rate η is inferred from Eq. (8.59),

$$\eta = \frac{R\,k^2 - \left[(1 + 2\,G\,Pe)\,n^2\,\pi^2 + (1 + G\,Pe)\,k^2\right]\left(n^2\,\pi^2 + k^2\right)}{\sigma\left[(1 + 2\,G\,Pe)\,n^2\,\pi^2 + (1 + G\,Pe)\,k^2\right]}\,, \tag{8.62}$$

and it depends explicitly on the form-drag parameter G.

Convective instability arises when the growth rate η becomes positive. Equation (8.62) implies that this is the case when

$$R > \frac{\left(\pi^2 + k^2\right)^2}{k^2} + G\,Pe\,\frac{\left(2\,\pi^2 + k^2\right)\left(\pi^2 + k^2\right)}{k^2}\,, \tag{8.63}$$

while the neutral stability condition is written as

$$R = \frac{\left(\pi^2 + k^2\right)^2}{k^2} + G\,Pe\,\frac{\left(2\,\pi^2 + k^2\right)\left(\pi^2 + k^2\right)}{k^2}\,. \tag{8.64}$$

Equations (8.63) and (8.64) are relative to modes with $n = 1$. In fact, these modes yield the least threshold for attaining positive growth rates, $\eta > 0$. In the limit $G \to 0$, that is switching off the form-drag effect, we recover the neutral stability function $R(k)$ determined for the Prats problem modelled by Darcy's law, given by Eq. (8.22). The effect of the form-drag coefficient is a stabilisation of the basic state. In fact, for a given k, the neutral stability value of R, defined by the right-hand side of Eq. (8.64), is an increasing function of the form-drag parameter G. The larger is G, the larger is the value of R needed for the onset of convective instability. The critical values of k and R are given by

$$k_c = \pi\left(\frac{1 + 2\,G\,Pe}{1 + G\,Pe}\right)^{1/4}\,, \quad R_c = \pi^2\left(\sqrt{1 + 2\,G\,Pe} + \sqrt{1 + G\,Pe}\right)^2\,. \tag{8.65}$$

As expected, in the Darcy's law limiting case, $G \to 0$, the critical values of k and R coincide with those expressed by Eq. (7.83).

Unlike the case where Darcy's law hold, when $G > 0$ the neutral stability condition (8.64) is influenced by the Péclet number, Pe, through the product $G\,Pe$. On the other hand, when the basic horizontal flow has a zero rate, $Pe \to 0$, the convective stability analysis of the Prats problem is not influenced by the form-drag effect. In this limit, the neutral stability condition and the critical values (k_c, R_c) coincide with those found for the Horton–Rogers–Lapwood problem, as we pointed out in Sect. 7.6.4.

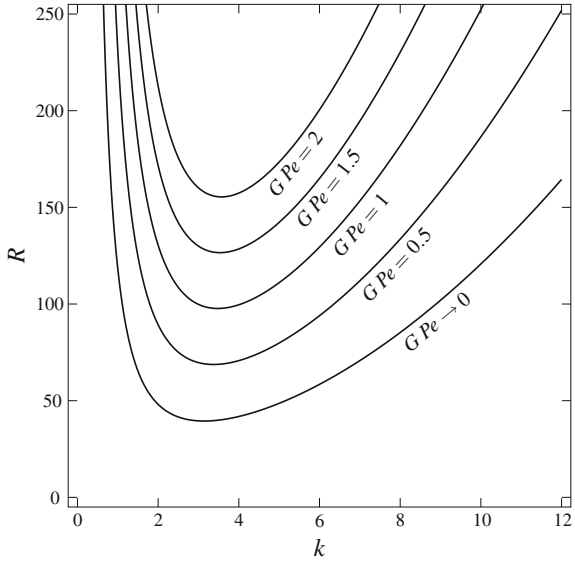

Fig. 8.6 Prats problem with form-drag effect: neutral stability curves in the (k, R) plane for different values of $G\,Pe$

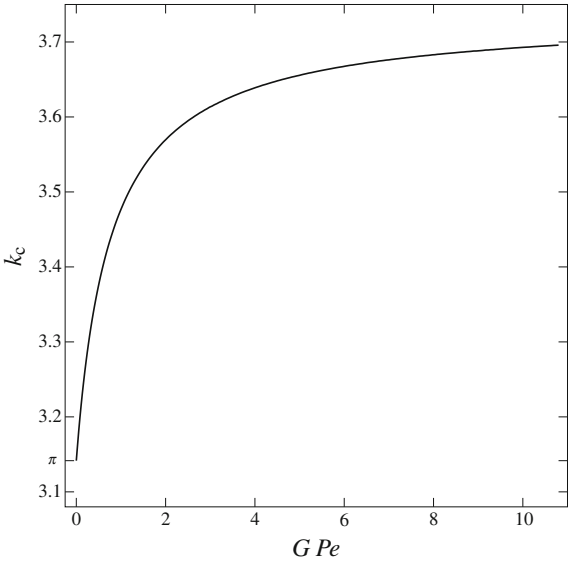

Fig. 8.7 Prats problem with form-drag effect: plot of k_c versus $G\,Pe$

A graphical representation of the neutral stability condition as described by Eq. (8.64) is provided in Fig. 8.6. The stabilising effect of the increasing parameter $G\,Pe$ is clearly illustrated in this figure.

Plots of k_c and R_c versus $G\,Pe$ are reported in Figs. 8.7 and 8.8. These figures clearly indicate that both the critical value of k and that of R, given by Eq. (8.65), increase with the intensification of the form-drag effect.

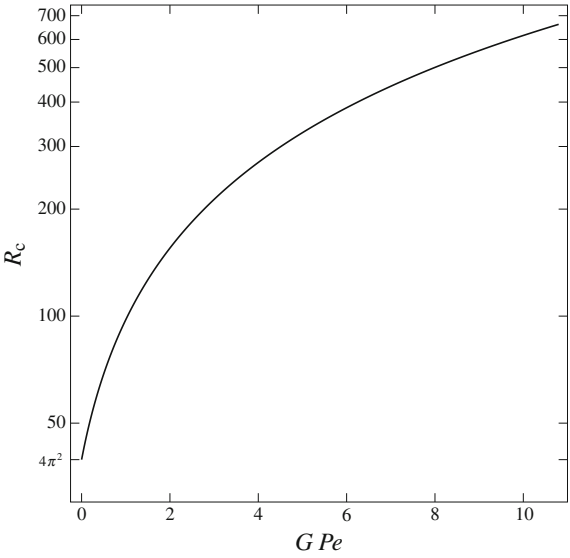

Fig. 8.8 Prats problem with form-drag effect: plot of R_c versus $G\,Pe$

8.3.3 Absolute Instability

The detection of the parametric transition to absolute instability involves the study of the asymptotic behaviour at large times for wave packet disturbances governed by Eq. (8.52). Such wave packets are still given by Eq. (8.23), with $\lambda(k)$ now given by Eqs. (8.56) and (8.59), namely

$$\sigma\,\lambda(k) = \frac{R\,k^2 - \left[(1+2\,G\,Pe)\,n^2\,\pi^2 + (1+G\,Pe)\,k^2\right]\left(n^2\,\pi^2 + k^2\right)}{(1+2\,G\,Pe)\,n^2\,\pi^2 + (1+G\,Pe)\,k^2} - \mathrm{i}\,k\,Pe\ , \tag{8.66}$$

with $n = 1, 2, 3, \ldots$. We follow the usual procedure, so that our first step is determining the saddle points of $\lambda(k)$. This means finding the roots of equation

$$\lambda'(k) = 0\ , \tag{8.67}$$

in the complex plane, $k \in \mathbb{C}$. On account of Eq. (8.66), Eq. (8.67) yields

$$\frac{2\,k\,R\,(1+2\,G\,Pe)\,n^2\pi^2}{\left[(1+2\,G\,Pe)\,n^2\pi^2 + (1+G\,Pe)\,k^2\right]^2} = 2\,k + \mathrm{i}\,Pe\ . \tag{8.68}$$

The solution of Eq. (8.68) to yield the saddle points and the evaluation of the associated values of R by setting $\Re(\lambda(k)) = 0$ goes much in the same manner as described in Sect. 8.2.4 relative to the case of Darcy's flow regime. When the form-drag effect is important, the position of the saddle point depends not only on Pe but also

on G. Unlike in the case of convective instability, where the neutral stability condition depends just on the product $G\,Pe$, here the two parameters G and Pe act independently, as made evident by Eqs. (8.67) and (8.68). What we concluded in Sect. 8.2.4 for the case $Pe = 0$ still holds for every $G > 0$. In fact, the form-drag contribution to the momentum balance is ineffective when $Pe = 0$. This means that Eq. (8.34) holds for every value of G if $Pe = 0$.

The evaluation of the saddle points depends significantly on G. Thus, with $n = 1$, $Pe = 10$ and $G = 0.05$, Eq. (8.36) is now replaced by

$$\begin{gathered} k_0 = \pm\, 3.78103 - \mathrm{i}\, 2.02087\ , \qquad R = 99.7984\ , \\ k_0 = \pm\, 2.13913 + \mathrm{i}\, 3.93823\ , \qquad R = -67.5161\ , \\ k_0 = \mathrm{i}\, 1.57971\ , \qquad R = 53.9911\ , \\ k_0 = -\,\mathrm{i}\, 6.82254\ , \qquad R = 33.9434\ . \end{gathered} \tag{8.69}$$

The determination of the saddle points identifying the transition to absolute instability is straightforward. We exclude those leading to a negative R, and those with R smaller than R_c. With $Pe = 10$ and $G = 0.05$, Eq. (8.65) yields $R_c = 68.7329$. Thus, we conclude that the saddle points which are relevant for the onset of absolute instability are $k_0 = \pm\, 3.78103 - \mathrm{i}\, 2.02087$ and that $R_a = 99.7984$.

Tracking the threshold conditions for absolute instability, with a given G, means recording the evolution of the saddle points as Pe increases above zero. We start from the pair given by Eq. (8.35), and we approach asymptotically the regime defined by the limit $Pe \to \infty$. We can study this asymptotic regime by recognising that the correct scaling of R at large Pe is not given by Eq. (8.38), but we have

$$R = \zeta\, G\, Pe^2\ , \tag{8.70}$$

instead.

Then, we keep the parameters ζ and G finite while $Pe \to \infty$, so that Eqs. (8.39) and (8.40) are now rewritten as

$$\frac{4\,k\,\zeta\,n^2\pi^2}{(2\,n^2\pi^2 + k^2)^2} = \mathrm{i}\ , \tag{8.71}$$

and

$$\frac{\sigma\,\lambda(k)}{Pe} = \frac{\zeta\,k^2}{2\,n^2\pi^2 + k^2} - \mathrm{i}\,k\ , \quad n = 1, 2, 3, \ \ldots\ . \tag{8.72}$$

One identifies the saddle points

$$k_0 = \pm \frac{\pi\, n}{2} \sqrt{\frac{7+\sqrt{17}}{2}} - \frac{\mathrm{i}\,\pi\, n}{2} \sqrt{\frac{5+3\sqrt{17}}{2}} \approx (\pm\, 3.70440 - \mathrm{i}\, 4.62910)\, n\ , \tag{8.73}$$

as associated with the positive value

$$\zeta = \frac{\pi\, n}{4} \sqrt{\frac{51\sqrt{17}-107}{2}} \approx 5.64390\, n\ . \tag{8.74}$$

Thus, we identify the threshold to absolute instability in the limiting case $Pe \to \infty$ by setting $n = 1$, namely

$$\frac{R_\mathrm{a}}{G\, Pe^2} = \frac{\pi}{4} \sqrt{\frac{51\sqrt{17}-107}{2}} \approx 5.64390\ . \tag{8.75}$$

The migration of the saddle points, as Pe increases above zero, starting from those found for $Pe = 0$, is illustrated in Fig. 8.9. The top left frame, relative to $G = 0$, is congruent with Fig. 8.2. A comparison with the top right frame of Fig. 8.9, relative to $G = 0.01$, highlights the discontinuity in the large Pe behaviour when G switches from 0 to an arbitrarily small, but positive, value. This is a consequence of the different behaviours defined by Eqs. (8.43) and (8.75). If $G = 0$, $R_\mathrm{a} \sim Pe$ when Pe is extremely large, while $R_\mathrm{a} \sim Pe^2$ when $G > 0$ and $Pe \gg 1$. In fact, the plots reported for $G = 0$ and $G = 0.01$ compare well for $Pe < 5$, while an increasing discrepancy is detected for higher values of Pe. The evolution of these plots as G becomes larger and larger is displayed in the other frames of Fig. 8.9, relative to $G = 0.02,\ 0.05,\ 0.1,\ 0.2$. What is common to all the frames with $G > 0$ is the position of the saddle points for $Pe = 0$ and $Pe \to \infty$.

Figure 8.10 shows the thresholds to convective instability, $R = R_\mathrm{c}$, and to absolute instability, $R = R_\mathrm{a}$, versus Pe. Different frames are relative to different values of G. We note that the gap between the values of R_a and R_c increases rapidly with Pe, starting from 0 when $Pe = 0$ and tending to infinity when $Pe \to \infty$. The frame for $G = 0$ is congruent with the plots provided in Fig. 8.4. As we already pointed out, this is the only case where R_c is independent of Pe. When $G > 0$, R_c increases with Pe approaching an asymptotic regime where

$$\frac{R_\mathrm{c}}{G\, Pe} = \pi^2 \left(1+\sqrt{2}\right)^2 \approx 57.5243\ , \tag{8.76}$$

when $Pe \gg 1$. Equation (8.76) is a consequence of Eq. (8.65). A comparison between Eqs. (8.75) and (8.76) reveals that R_a grows more rapidly than R_c for large values of Pe, so that

$$\frac{R_\mathrm{a}}{R_\mathrm{c}} = \frac{\left(3\sqrt{2}-4\right)\sqrt{51\sqrt{17}-107}}{8\,\pi}\, Pe \approx 0.0981134\, Pe\ . \tag{8.77}$$

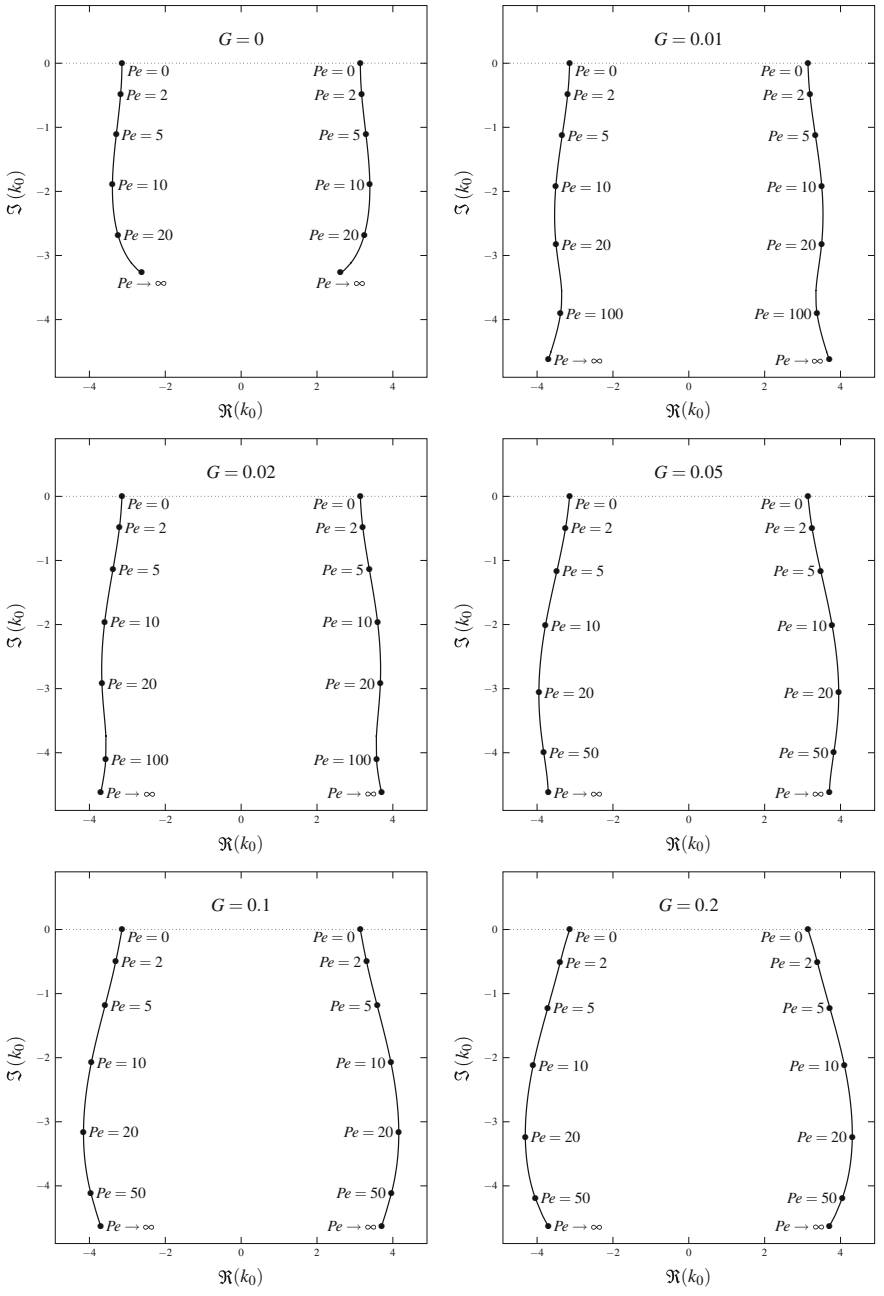

Fig. 8.9 Prats problem with form-drag effect: migration of the pertinent saddle points, with increasing values of Pe and fixed values of G, for the threshold to absolute instability

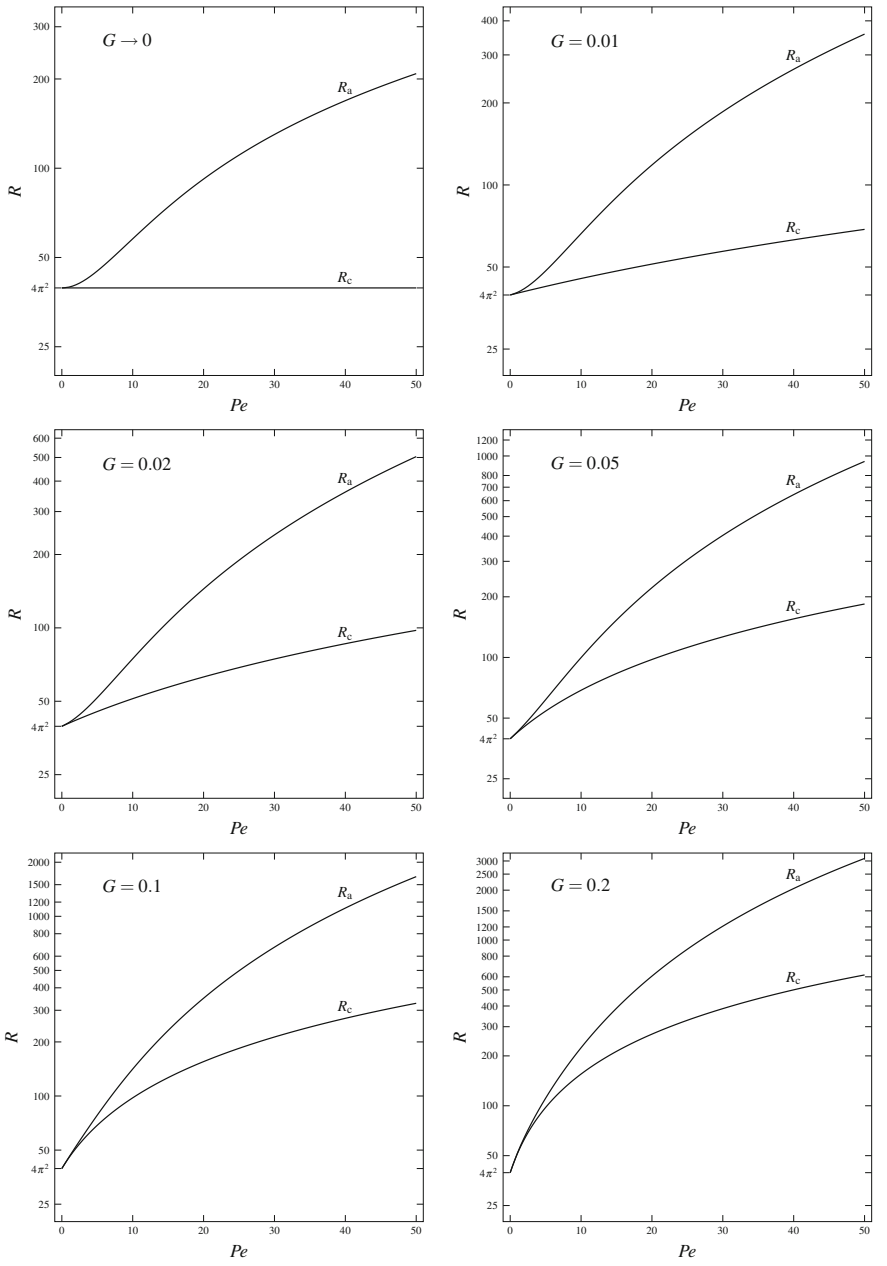

Fig. 8.10 Prats problem with form-drag effect: thresholds R_c and R_a to convective and absolute instabilities versus Pe, with increasing values of G

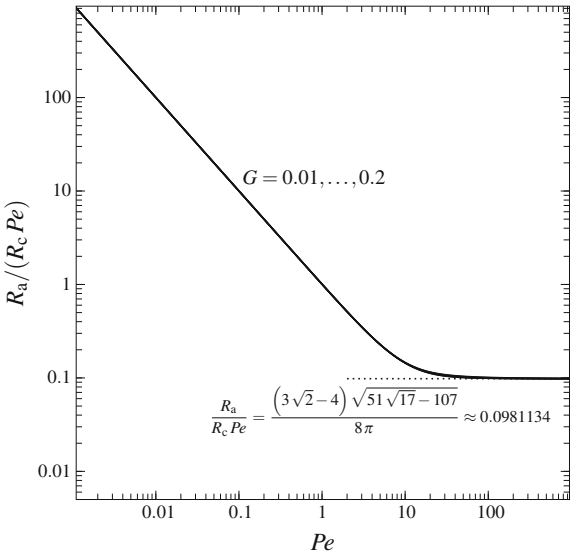

Fig. 8.11 Prats problem with form-drag effect: plots of $R_a/(R_c\,Pe)$ versus Pe within the range $0.01 \leqslant G \leqslant 0.2$

Equation (8.77) is to be intended as an asymptotic formula. Evidently, it does not make any good sense if Pe is smaller than approximately 10.19, as it would predict $R_a < R_c$, which is absurd. Interestingly enough, Eq. (8.77) reveals that the asymptotic behaviour of the ratio R_a/R_c is independent of $G > 0$.

Interestingly enough, on account of Eqs. (7.83) and (8.43), relative to the case $G = 0$, Eq. (8.77) does not hold true in the Darcy's flow limit, as we have

$$\frac{R_a}{R_c} = \frac{\sqrt{51\sqrt{17}-107}}{32\,\pi}\,Pe \approx 0.101089\,Pe\ . \tag{8.78}$$

In practice, the discrepancy between Eq. (8.78), for $G = 0$, and Eq. (8.77), for any $G > 0$, is not very strong, but it is symptomatic of the difference in the asymptotic behaviour detected in these cases when $Pe \gg 1$.

Figure 8.11 displays the trend of $R_a/(R_c\,Pe)$ versus Pe for different values of G within the range $0.01 \leqslant G \leqslant 0.2$. The dependence on G is barely visible, and it is concentrated in a narrow region between $Pe = 10$ and $Pe = 100$. This is an interesting, to some extent expected, behaviour. In fact, when $Pe \ll 1$, one has the asymptotic formula $R_a/(R_c\,Pe) = 1/Pe$, which is independent of G exactly as it happens with Eq. (8.77) for the limiting case $Pe \gg 1$. That a slight dependence on G is indeed present is better illustrated in Fig. 8.12, where the same data reported in Fig. 8.11 are zoomed in the range $10 \leqslant Pe \leqslant 100$.

A check that the holomorphy requirement is satisfied in the limiting case $Pe \to \infty$ is illustrated in Fig. 8.13. This figure displays the behaviour of $\Re(\lambda)$ as a function of the real and imaginary parts of k. Much in the same manner as Fig. 8.3, we reckon that Fig. 8.13 suggests the possibility of a regular deformation of the path $\Im(k) = 0$

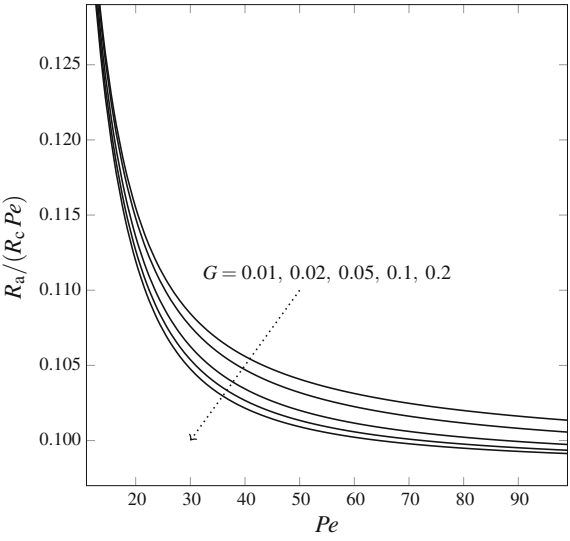

Fig. 8.12 Prats problem with form-drag effect: plots of $R_a/(R_c\,Pe)$ versus Pe within the range $0.01 \leqslant G \leqslant 0.2$

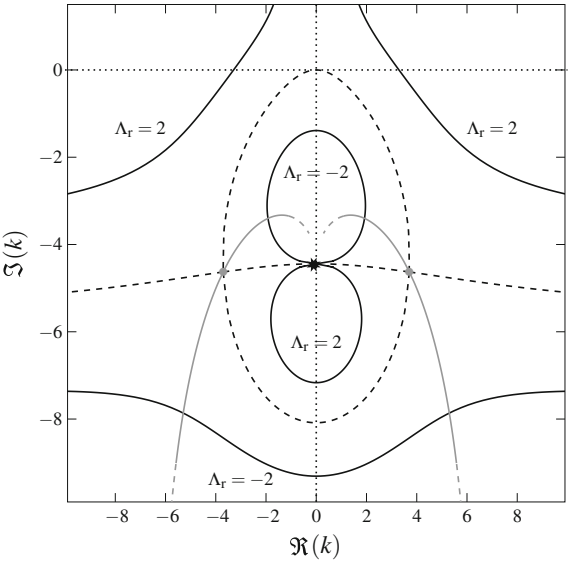

Fig. 8.13 Prats problem with form-drag effect: map of the isolines of $\sigma\,\Re(\lambda)/Pe = \Lambda_r$ (black solid lines) for the limiting case $Pe \to \infty$ with $\zeta = R_a/(G\,Pe^2) = 5.64390$. The dashed black lines are for $\Lambda_r = 0$. The grey dots are the saddle points, while the grey lines are the lines of steepest descent. The black asterisk denotes the singularity of $\lambda(k)$ at $k = -\mathrm{i}\,\pi\,\sqrt{2}$

so that the saddle points k_0, given by Eq. (8.73), are locally crossed along lines of steepest descent. By the adjective "regular", we mean that no singularity of $\Re(\lambda)$ is swept in the deformation, so that the region in the complex plane between $\Im(k) = 0$ and the deformed path does not include any singularity. We need to move along paths of steepest descent only in a neighbourhood of each saddle point. In fact, the Gaussian approximation of the integrand, in the wave packet representation (8.23), is rapidly damped as we depart from the saddle point. We recall that, as illustrated

in Sect. 3.5.3, the Gaussian approximation (3.159) of a time-dependent integral is the core of the steepest-descent method for capturing the large-time behaviour of the integral. In Fig. 8.13, just one singularity is displayed, namely $k = -\mathrm{i}\,\pi\,\sqrt{2}$, as one expects by inspecting equation (8.72) with $n = 1$.

8.4 Moving to Three Dimensions

In the formulation of the Prats problem, discussed in Sect. 8.2, we adopted a two-dimensional scheme disregarding the dependence of all physical fields on the spanwise coordinate y. Such a scheme is legitimate as far as the porous channel has a very small width H in the y-direction, namely $H/L \ll 1$. Assuming non-infinitesimal values of H/L means relaxing the assumption of two-dimensional flow. In this case, the velocity, pressure and temperature fields are to be considered as functions of (x, y, z, t). We rely on Darcy's law, for the sake of simplicity, namely on Eq. (7.61), where we consider the effect of viscous dissipation as negligible.

One may envisage a lateral confinement along the spanwise y-direction with adiabatic and impermeable sidewalls. Hence, a streamfunction formulation is out of the question, as it is feasible only for two-dimensional flows, while a pressure formulation is possible. Starting from Eq. (7.61), where we neglect the viscous dissipation term $\nu\, u_j\, u_j/(K\, c)$, we evaluate the divergence of the local momentum balance equation and we employ the local mass balance equation. Thus, in a dimensionless formulation, we write

$$\frac{\partial^2 P}{\partial x^2} + \frac{\partial^2 P}{\partial y^2} + \frac{\partial^2 P}{\partial z^2} - R\,\frac{\partial T}{\partial z} = 0\,,$$

$$\sigma\,\frac{\partial T}{\partial t} - \frac{\partial P}{\partial x}\,\frac{\partial T}{\partial x} - \frac{\partial P}{\partial y}\,\frac{\partial T}{\partial y} - \left[\frac{\partial P}{\partial z} - R\,(T - r)\right]\frac{\partial T}{\partial z} = \frac{\partial^2 T}{\partial x^2} + \frac{\partial^2 T}{\partial y^2} + \frac{\partial^2 T}{\partial z^2}\,. \tag{8.79}$$

where $r = (T_0 - T_2)/(T_1 - T_2)$ is a parameter depending on the choice of the reference temperature, T_0, for the Oberbeck–Boussinesq approximation.

In Eq. (8.79), a scaling consistent with Eq. (8.1) has been implicitly adopted and we allowed for the definition of the dimensionless quantity P, namely

$$\frac{K}{\mu\,\alpha}\,P \to P\,. \tag{8.80}$$

The basic solution with a uniform velocity profile, given by Eqs. (8.8)–(8.10), still holds. It can be reformulated as

$$\frac{\partial P_\mathrm{b}}{\partial x} = -Pe\ , \quad \frac{\partial P_\mathrm{b}}{\partial y} = 0\ , \quad \frac{\partial P_\mathrm{b}}{\partial z} = R\,(1 - z - r)\ , \quad T_\mathrm{b} = 1 - z\ . \tag{8.81}$$

We note that Eq. (8.81) reflects the adiabatic and impermeable nature of the sidewalls, as one must satisfy the boundary conditions $\partial T/\partial y = 0$ and $\partial P/\partial y = 0$. Hereafter, we will assume the sidewalls to be placed at the dimensionless positions $y = 0, \tau$, where

$$\tau = \frac{H}{L}\ . \tag{8.82}$$

The small perturbations of the basic state (8.81) are defined as

$$P = P_\mathrm{b} + \varepsilon\,\Pi\ , \qquad T = T_\mathrm{b} + \varepsilon\,\Theta\ . \tag{8.83}$$

On substituting Eq. (8.83) into Eq. (8.79) and neglecting the terms $O(\varepsilon^2)$ leads to the governing equations for the three-dimensional perturbations,

$$\begin{gathered}\frac{\partial^2 \Pi}{\partial x^2} + \frac{\partial^2 \Pi}{\partial y^2} + \frac{\partial^2 \Pi}{\partial z^2} - R\,\frac{\partial \Theta}{\partial z} = 0\ , \\ \sigma\ \frac{\partial \Theta}{\partial t} + Pe\,\frac{\partial \Theta}{\partial x} + \frac{\partial \Pi}{\partial z} - R\,\Theta = \frac{\partial^2 \Theta}{\partial x^2} + \frac{\partial^2 \Theta}{\partial y^2} + \frac{\partial^2 \Theta}{\partial z^2}\ .\end{gathered} \tag{8.84}$$

Instead of Eq. (8.12), the boundary conditions are now written as

$$\begin{aligned} y = 0, \tau: &\qquad \frac{\partial \Pi}{\partial y} = 0\ , \quad \frac{\partial \Theta}{\partial y} = 0\ , \\ z = 0, 1: &\qquad \frac{\partial \Pi}{\partial z} = 0\ , \quad \Theta = 0\ . \end{aligned} \tag{8.85}$$

We note that Eqs. (8.84) and (8.85) do not depend on the reference temperature parameter $r = (T_0 - T_2)/(T_1 - T_2)$. This means that the stability analysis is not influenced by the choice of T_0 and, hence, by the value of r. This is an important fact regarding instability in a horizontal channel. We anticipate that the conclusion becomes quite the opposite if we consider flow in a vertical porous channel, as it will become clear in Sect. 9.2.

The perturbations (Π, Θ) are now written as wave packets by employing the Fourier transform,

$$\tilde{\Pi}(k, y, z, t) = \frac{1}{\sqrt{2\pi}} \int_{-\infty}^{\infty} e^{-\mathrm{i}\,k\,x}\,\Pi(x, y, z, t)\ \mathrm{d}\,x\ ,$$

$$\Pi(x,y,z,t) = \frac{1}{\sqrt{2\pi}} \int_{-\infty}^{\infty} e^{\mathrm{i}\,k\,x}\,\tilde{\Pi}(k,y,z,t)\,\mathrm{d}\,k\ ,$$

$$\tilde{\Theta}(k,y,z,t) = \frac{1}{\sqrt{2\pi}} \int_{-\infty}^{\infty} e^{-\mathrm{i}\,k\,x}\,\Theta(x,y,z,t)\,\mathrm{d}\,x\ ,$$

$$\Theta(x,y,z,t) = \frac{1}{\sqrt{2\pi}} \int_{-\infty}^{\infty} e^{\mathrm{i}\,k\,x}\,\tilde{\Theta}(k,y,z,t)\,\mathrm{d}\,k\ . \tag{8.86}$$

We can now separate the dependence on y and z, by writing

$$\tilde{\Pi}(k,y,z,t) = \sum_{\ell=0}^{\infty}\sum_{n=1}^{\infty} \tilde{\Pi}_{\ell,n}(t)\,\cos\left(\frac{\ell\,\pi\,y}{\tau}\right)\cos(n\,\pi\,z)\ ,$$

$$\tilde{\Theta}(k,y,z,t) = \sum_{\ell=0}^{\infty}\sum_{n=1}^{\infty} \tilde{\Theta}_{\ell,n}(t)\,\cos\left(\frac{\ell\,\pi\,y}{\tau}\right)\sin(n\,\pi\,z)\ . \tag{8.87}$$

We easily reckon that Eq. (8.87), when substituted in Eq. (8.86), allows one to infer that the boundary conditions at $y = 0, \tau$ and $z = 0, 1$ declared in Eq. (8.85) are identically satisfied.

The three-dimensional formulation expressed by Eq. (8.87) includes the two-dimensional modes discussed in Sect. 8.2. Such modes are, in fact, those corresponding to $\ell = 0$ as this selection suppresses any dependence on y.

By applying the Fourier transform to Eq. (8.84), one obtains

$$\left(n^2\,\pi^2 + \frac{\ell^2\,\pi^2}{\tau^2} + k^2\right)\tilde{\Pi}_{\ell,n} + n\,\pi\,R\,\tilde{\Theta}_{\ell,n} = 0\ ,$$

$$\left(n^2\,\pi^2 + \frac{\ell^2\,\pi^2}{\tau^2} + k^2\right)\tilde{\Theta}_{\ell,n} + \sigma\,\frac{\mathrm{d}\,\tilde{\Theta}_{\ell,n}}{\mathrm{d}\,t} + \mathrm{i}\,k\,Pe\,\tilde{\Theta}_{\ell,n} - n\,\pi\,\tilde{\Pi}_{\ell,n} - R\,\tilde{\Theta}_{\ell,n} = 0\ , \tag{8.88}$$

where Eq. (8.87) has been taken into account.

Equations (8.88) can be solved by writing

$$\tilde{\Pi}_{\ell,n}(t) = \tilde{\Pi}_{\ell,n}(0)\,\mathrm{e}^{\lambda(k)\,t}\ ,\quad \tilde{\Theta}_{\ell,n}(t) = -\frac{n^2\,\pi^2 + \dfrac{\ell^2\,\pi^2}{\tau^2} + k^2}{n\,\pi\,R}\,\tilde{\Pi}_{\ell,n}(0)\,\mathrm{e}^{\lambda(k)\,t}\ , \tag{8.89}$$

with the dispersion relation now given by

$$\sigma\,\lambda(k) = \frac{R\left(\dfrac{\ell^2\,\pi^2}{\tau^2} + k^2\right) - \left(n^2\pi^2 + \dfrac{\ell^2\,\pi^2}{\tau^2} + k^2\right)^2}{n^2\pi^2 + \dfrac{\ell^2\,\pi^2}{\tau^2} + k^2} - \mathrm{i}\,k\,Pe\ ,$$

$$n = 1, 2, 3, \ \ldots\ , \quad \ell = 0, 1, 2, \ \ldots\ . \tag{8.90}$$

8.4.1 Convective Instability

Following the usual procedure, in the analysis of convective instability, we must remember that $\lambda = \eta - \mathrm{i}\,\omega$, where η is the growth rate of the normal mode and ω is its angular frequency. Thus, by considering the real part and the imaginary part of the dispersion relation (8.90), we obtain

$$\eta = \frac{R\,\kappa^2 - (n^2\pi^2 + \kappa^2)^2}{\sigma\left(n^2\pi^2 + \kappa^2\right)}\ , \quad \omega = \frac{k\,Pe}{\sigma}\ , \quad n = 1, 2, 3, \ \ldots\ , \tag{8.91}$$

where

$$\kappa^2 = \frac{\ell^2\,\pi^2}{\tau^2} + k^2\ , \quad \ell = 0, 1, 2, \ \ldots\ . \tag{8.92}$$

A comparison between Eq. (8.91) and its two-dimensional counterpart (8.20) immediately suggests that the neutral stability condition has formally the same expression as for the two-dimensional case. More precisely, it is given by Eq. (8.22) with parameter κ instead of the wave number k,

$$R = \frac{(\pi^2 + \kappa^2)^2}{\kappa^2}\ . \tag{8.93}$$

This means that the onset of convective instability is still triggered by the $n = 1$ modes. Hence, the minimum of the neutral stability curve is now expressed as

$$\kappa_\mathrm{c} = \pi\ , \qquad R_\mathrm{c} = 4\,\pi^2\ , \tag{8.94}$$

which replaces Eq. (7.83). There is just one difference: κ appears instead of k. This means that, in general, there is not only a two-dimensional mode ($\ell = 0$) as a possible source of convective instability. Obviously, for such mode, one recovers the result found with the two-dimensional analysis, namely $k_\mathrm{c} = \pi$, consistently with Eq. (7.83). However, with three-dimensional modes ($\ell \neq 0$), one has

$$k_\mathrm{c} = \pi\sqrt{1 - \frac{\ell^2}{\tau^2}}\ . \tag{8.95}$$

Evidently, a mode with $\ell = 1$ can be involved only if $\tau \geqslant 1$, a mode with $\ell = 2$ can be involved only if $\tau \geqslant 2$, and so on. This simple observation is coherent with our statement that a two-dimensional analysis is a reliable model when $\tau = H/L$ is small enough. In particular, the two-dimensional nature of the critical mode, with $\kappa_c = k_c = \pi$, arises when $\tau < 1$ as we can only have $\ell = 0$ in this case, meaning y independent modes. When $1 \leqslant \tau < 2$, we have two modes satisfying the criticality condition expressed by Eq. (8.95), namely

$$\ell = 0 \,, \quad k_c = \pi \,,$$

$$\ell = 1 \,, \quad k_c = \pi \sqrt{1 - \frac{1}{\tau^2}} \,. \tag{8.96}$$

When $2 \leqslant \tau < 3$, we have three modes, namely

$$\ell = 0 \,, \quad k_c = \pi \,,$$

$$\ell = 1 \,, \quad k_c = \pi \sqrt{1 - \frac{1}{\tau^2}} \,,$$

$$\ell = 2 \,, \quad k_c = \pi \sqrt{1 - \frac{4}{\tau^2}} \,. \tag{8.97}$$

When $3 \leqslant \tau < 4$, we have four modes, and so forth.

The plurality of possible modes triggering the onset of convective instability widens as τ increases. The simplest case being that with $\tau < 1$ where only the two-dimensional mode with $k_c = \pi$ is involved.

The completely different types of two-dimensional modes potentially driving convective instability are those with $k = 0$ and $\ell \neq 0$. Such modes were not included in the analysis conveyed in Sect. 8.2.3 as they display a dependence on the pair of coordinates (y, z). Furthermore, the modes envisaged in Sect. 8.2.3 do not lead to any instability when $k \to 0$, as testified by the singularity at $k = 0$ in the right-hand side of Eq. (8.22). Equations (8.92) and (8.93) depict a different situation, with the neutral stability value of R being a function of τ for every $\ell \neq 0$ and $k = 0$. In particular, there exists a range of the aspect ratio τ where the modes with $\ell = 1$ are those leading to the lowest neutral stability value of R. There exists a neighbouring range of τ where the modes with $\ell = 2$ prevail, and so forth. The transition from the ℓth mode to the $(\ell + 1)$th mode in the neutral stability condition with an increasing aspect ratio τ is illustrated in Fig. 8.14. This figure shows that, as τ increases, larger and larger values are involved in the onset of convective instability. From Eqs. (8.92) and (8.93), one may infer that the transition value of τ from the range where the ℓth mode triggers the onset of convective instability to the range where the $(\ell + 1)$th mode prevails is

$$\tau = \sqrt{\ell \, (\ell + 1)} \,. \tag{8.98}$$

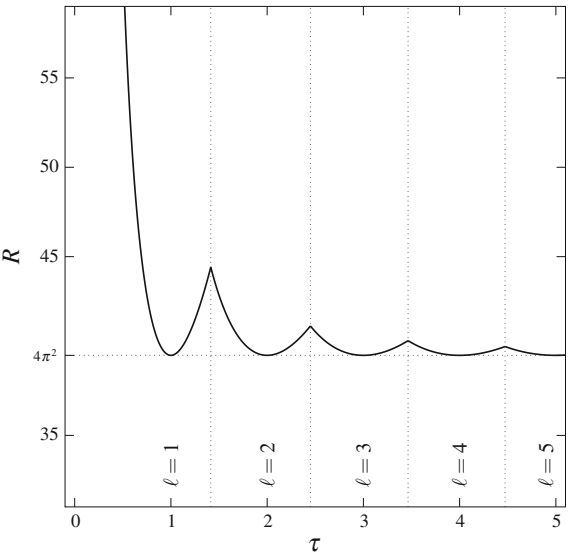

Fig. 8.14 Three-dimensional analysis of the Prats problem: the neutral stability condition for the $k = 0$ modes in the (τ, R) plane (solid line). The vertical dotted lines mark the transition between different ℓ modes. The horizontal dotted line denotes the critical value of R

We note that, on account of Eqs. (8.92) and (8.93), the critical condition $R = R_c = 4\,\pi^2$ occurs with $k = 0$ modes for any $\tau = \ell$, where $\ell = 1, 2, 3, \ldots$. Hence, the neutral stability curve displayed in Fig. 8.14 displays a sequence of minima for $\tau = 1, 2, 3, \ldots$. This conclusion reflects the geometry of the preferred convection cells for the onset of convective instability, i.e., the square geometry. This aspect was pointed out in Sect. 7.8 and illustrated in Fig. 7.13, with reference to the Horton–Rogers–Lapwood problem with impermeable and isothermal boundaries.

8.4.2 Absolute Instability

The analysis of the absolute instability is to be based on the dispersion relation (8.90) and on the derivative of $\lambda(k)$. As usual, $\lambda'(k)$ is to be set equal to zero in order to determine the saddle points, whereas the condition $\Re(\lambda(k)) = 0$ serves to establish the associated value of R. Thus, starting from Eq. (8.90), the condition $\lambda'(k) = 0$ reads

$$\frac{2\,k\,R\,n^2\pi^2}{\left(n^2\pi^2 + \dfrac{\ell^2\,\pi^2}{\tau^2} + k^2\right)^2} = 2\,k + \mathrm{i}\,Pe\ . \tag{8.99}$$

Equations (8.90) and (8.99), differently from Eqs. (8.25) and (8.27), display a dependence on the ratio ℓ/τ. Any value of such ratio is effectively a real positive number that may correspond to different ℓ modes and to different aspect ratios τ. Relatively to the absolute instability analysis, it is quite evident that the $\ell = 0$ modes are to

be considered equivalent to $\ell \neq 0$ modes having an infinite aspect ratio τ. In other words, for $\tau \to \infty$ and for each Péclet number, Pe, the absolute instability threshold, R_a, coincides with that evaluated for the two-dimensional case reported in Sect. 8.2.4.

The two-dimensional case is represented by $\ell/\tau = 0$. Then, we have to test the behaviour of the saddle points k_0 and to the corresponding values of R when ℓ/τ increases above 0. We consider the Péclet number $Pe = 10$ and $n = 1$, so that the saddle points for the two-dimensional case $\ell/\tau = 0$ are expressed by Eq. (8.36). If we take $\ell/\tau = 0.01$, we obtain

$$\begin{aligned} k_0 &= \pm\, 3.39291 - \mathrm{i}\, 1.89310\,, \qquad R = 57.8045\,, \\ k_0 &= \pm\, 1.84689 + \mathrm{i}\, 3.39165\,, \qquad R = -36.0948\,, \\ k_0 &= \mathrm{i}\, 1.51479\,, \qquad R = 25.0108\,, \\ k_0 &= -\mathrm{i}\, 6.51499\,, \qquad R = 25.0006\,, \\ k_0 &= \mathrm{i}\, 0.000500177\,, \qquad R = 98690.8\,. \end{aligned} \tag{8.100}$$

From Eqs. (8.36) and (8.100), we conclude that there is a little difference in the saddle points for $\ell/\tau = 0$ and those for $\ell/\tau = 0.01$. There is indeed a new one, purely imaginary and close to the origin of the k plane, where R is extremely large, $R = 98690.8$. We expect that such saddle point is moved to the origin, with $R \to \infty$, when $\ell/\tau \to 0$. This is the reason why the two-dimensional analysis did not reveal any such point. The other saddle points reported in Eq. (8.100) can be easily put in correspondence with those listed in Eq. (8.36). The numerical values are slightly altered with respect to the two-dimensional case. The interesting fact is that there is no good candidate for the threshold value R_a that can be gathered from Eq. (8.100) to replace that obtained with the two-dimensional analysis, namely $R_a = 57.8036$. In fact, the change from $\ell/\tau = 0$ to $\ell/\tau = 0.01$ does not provide any saddle point whose corresponding R is both larger than $R_c = 4\,\pi^2$ and smaller than the two-dimensional threshold value for absolute instability, $R_a = 57.8036$. Just the same happens if we further increase to $\ell/\tau = 0.1$. We get

$$\begin{aligned} k_0 &= \pm\, 3.38719 - \mathrm{i}\, 1.90297\,, \qquad R = 57.9011\,, \\ k_0 &= \pm\, 1.84401 + \mathrm{i}\, 3.40539\,, \qquad R = -36.2194\,, \\ k_0 &= \mathrm{i}\, 1.50091\,, \qquad R = 26.1248\,, \\ k_0 &= -\mathrm{i}\, 6.52134\,, \qquad R = 25.0581\,, \\ k_0 &= \mathrm{i}\, 0.0518395\,, \qquad R = 980.612\,. \end{aligned} \tag{8.101}$$

The outcome from Eqs. (8.100) and (8.101) is that there is no good candidate that emerges from the three-dimensional analysis for the replacement of our threshold for absolute instability, $R_a = 57.8036$. One can check the saddle points for larger values of ℓ/τ. With $\ell/\tau = 1$, we find

$$\begin{aligned} k_0 &= \pm 3.06328 - \mathrm{i}\, 2.81016 \,, \qquad R = 68.5544 \,, \\ k_0 &= \pm 1.65805 + \mathrm{i}\, 4.59899 \,, \qquad R = -47.3176 \,, \\ k_0 &= -\mathrm{i}\, 7.16371 \,, \qquad R = 30.5193 \,. \end{aligned} \tag{8.102}$$

With $\ell/\tau = 10$, we obtain

$$\begin{aligned} k_0 &= \pm 0.821325 + \mathrm{i}\, 31.5818 \,, \qquad R = -315.833 \,, \\ k_0 &= -\mathrm{i}\, 32.3801 \,, \qquad R = 228.491 \,, \\ k_0 &= -\mathrm{i}\, 30.4151 \,, \qquad R = 435.856 \,, \\ k_0 &= -\mathrm{i}\, 5.05459 \,, \qquad R = 1032.32 \,. \end{aligned} \tag{8.103}$$

Finally, with $\ell/\tau = 100$ we have

$$\begin{aligned} k_0 &= \pm 0.278039 + \mathrm{i}\, 314.175 \,, \qquad R = -3141.75 \,, \\ k_0 &= -\mathrm{i}\, 314.442 \,, \qquad R = 2811.27 \,, \\ k_0 &= -\mathrm{i}\, 313.876 \,, \qquad R = 3511.08 \,, \\ k_0 &= -\mathrm{i}\, 5.00050 \,, \qquad R = 98740.8 \,. \end{aligned} \tag{8.104}$$

The conclusion drawn from Eqs. (8.100)–(8.104) is that, no matter how much we increase the value of ℓ/τ above zero, the three-dimensional analysis does not alter the findings of the two-dimensional analysis. The correct threshold to absolute instability for $Pe = 10$ is detected by setting $\ell/\tau = 0$, namely $R_a = 57.8036$.

The same type of analysis can be carried out with different values of the Péclet number, Pe. Table 8.2 is relative to $Pe = 5$, while Table 8.3 reports the saddle points for $Pe = 20$.

Both these tables allow one to reach the same conclusion declared for $Pe = 10$. On inspecting the behaviour of the saddle points by increasing the value of ℓ/τ above zero, one does not detect any case where the value of R corresponding to a given saddle point is both larger or equal to R_c and smaller than the value of R_a estimated with the two-dimensional analysis ($\ell/\tau = 0$). This means that, whatever is the value of Pe and τ, the three-dimensional analysis does not provide any change with respect to the findings of the two-dimensional analysis, succinctly reported in Table 8.1. In

Table 8.2 Three-dimensional analysis of the Prats problem: saddle points of $\lambda(k)$ and corresponding values of R for $Pe = 5$, $n = 1$ and different values of ℓ/τ

ℓ/τ	k_0	R
0	$\pm\,3.29255 - \mathrm{i}\,1.12014$	45.0277
	$\pm\,1.51430 + \mathrm{i}\,3.36050$	−17.3610
	$\mathrm{i}\,2.13114$	6.25
	$-\mathrm{i}\,4.63114$	6.25
0.01	$\pm\,3.29245 - \mathrm{i}\,1.12022$	45.0281
	$\pm\,1.51428 + \mathrm{i}\,3.36064$	−17.3617
	$\mathrm{i}\,2.13122$	6.25136
	$-\mathrm{i}\,4.63126$	6.25029
	$\mathrm{i}\,0.000250041$	98709.5
0.1	$\pm\,3.28256 - \mathrm{i}\,1.12803$	45.0689
	$\pm\,1.51173 + \mathrm{i}\,3.37459$	−17.4274
	$\mathrm{i}\,2.13932$	6.38733
	$-\mathrm{i}\,4.64281$	6.27873
	$\mathrm{i}\,0.0254128$	1000.38
1	$\pm\,2.60121 - \mathrm{i}\,1.96765$	50.8973
	$\pm\,1.34343 + \mathrm{i}\,4.57619$	−23.1883
	$-\mathrm{i}\,5.67901$	8.87912
10	$\pm\,0.601695 + \mathrm{i}\,31.5779$	−157.892
	$-\mathrm{i}\,32.0817$	98.1192
	$-\mathrm{i}\,30.7344$	253.875
	$-\mathrm{i}\,2.52575$	1013.18
100	$\pm\,0.197378 + \mathrm{i}\,314.175$	−1570.88
	$-\mathrm{i}\,314.359$	1341.65
	$-\mathrm{i}\,313.960$	1839.27
	$-\mathrm{i}\,2.50025$	98722.0

other words, the value of R_a for a given Pe is independent of the aspect ratio τ. This conclusion is in no way the result of a formal mathematical proof, but rather the outcome of an inductive reasoning based on numerical data.

8.4.3 On the Different Meanings of Three Dimensionality

The three-dimensional nature of the instability has been modelled by assuming a pair of plane-parallel sidewalls bounding laterally the horizontal flow. The whole analysis has been based on the assumption that the sidewalls are adiabatic and impermeable.

There are two levels of arbitrariness in our model of three dimensionality. One is the existence and the plane-parallel geometry of the lateral boundaries. The other is the type of boundary conditions assumed at the sidewalls.

Table 8.3 Three-dimensional analysis of the Prats problem: saddle points of $\lambda(k)$ and corresponding values of R for $Pe = 20$, $n = 1$ and different values of ℓ/τ

ℓ/τ	k_0	R
0	$\pm\,3.24476 - \mathrm{i}\,2.68308$	91.9528
	$\pm\,2.13593 + \mathrm{i}\,3.38608$	−74.7989
	$\mathrm{i}\,0.905049$	100
	$-\mathrm{i}\,10.9050$	100
0.01	$\pm\,3.24472 - \mathrm{i}\,2.68320$	91.9548
	$\pm\,2.13590 + \mathrm{i}\,3.38622$	−74.8013
	$\mathrm{i}\,0.904350$	100.121
	$-\mathrm{i}\,10.9051$	100.001
	$\mathrm{i}\,0.00100112$	98615.7
0.1	$\pm\,3.24132 - \mathrm{i}\,2.69522$	92.1583
	$\pm\,2.13278 + \mathrm{i}\,3.39985$	−75.0395
	$\mathrm{i}\,0.822457$	115.111
	$-\mathrm{i}\,10.9069$	100.083
	$\mathrm{i}\,0.113910$	891.598
1	$\pm\,3.10130 - \mathrm{i}\,3.76867$	112.140
	$\pm\,1.93786 + \mathrm{i}\,4.59367$	−96.5459
	$-\mathrm{i}\,11.1053$	108.208
10	$\pm\,1.08953 + \mathrm{i}\,31.5869$	−631.828
	$-\mathrm{i}\,32.8959$	513.232
	$-\mathrm{i}\,29.8254$	775.094
	$-\mathrm{i}\,10.1388$	1109.05
100	$\pm\,0.390162 + \mathrm{i}\,314.175$	−6283.50
	$-\mathrm{i}\,314.562$	5812.17
	$-\mathrm{i}\,313.756$	6793.05
	$-\mathrm{i}\,10.0010$	98815.8

The absence of lateral boundaries can be intended as a limiting case of the analysis carried out so far, with $\tau \to \infty$. There is a spanwise wave number given by $k_s = \ell\,\pi/\tau$ that displays a discrete spectrum for every finite τ. However, in the limiting case, the spectrum becomes continuous as the distance between two neighbouring wave numbers, π/τ, tends to zero when $\tau \to \infty$. Therefore, the normal modes defined by Eqs. (8.86) and (8.87) yield a situation where such modes propagate along a direction described by a wave vector with components (k, k_s) lying in the horizontal (x, y) plane. Thus, the lateral boundaries, when moved to infinity, are ineffective for the convective and absolute stability analysis.

The role of the boundary conditions prescribed at the lateral boundaries, when τ is finite, is another matter. In fact, these boundary conditions are quite important in defining the y-dependent eigenfunctions to be used in Eq. (8.87) instead of the cosine, as well as their corresponding eigenvalues to be employed instead of $k_s = \ell\,\pi/\tau$. To a far deeper extent, the boundary conditions prescribed at the sidewalls

are of paramount importance in assessing the type of stationary flow solution to be considered as the basic state. Not necessarily any possible model of sidewalls can be compatible with the uniform flow endowed with a purely vertical temperature gradient, as described by Eq. (8.81). The nature of the basic state may be deeply influenced by the temperature and pressure constraints prescribed on the lateral boundaries. The sidewalls assumed in the stability analysis carried out in Sects. 8.4.1 and 8.4.2 are a natural expression of the heating-from-below scenario, where the onset of convection cells is a consequence of the vertical temperature gradient induced by the thermal forcing at the lower boundary wall.

References

1. Alves LSB, Barletta A (2015) Convective to absolute instability transition in the Prats flow of a power-law fluid. Int J Thermal Sci 94:270–282
2. Barletta A, Alves LSB (2017) Absolute instability: a toy model and an application to the Rayleigh-Bénard problem with horizontal flow in porous media. Int J Heat Mass Transf 104:438–455
3. Barletta A, Celli M (2017) Convective to absolute instability transition in a horizontal porous channel with open upper boundary. Fluids 2:1–33
4. Brevdo L (2009) Three-dimensional absolute and convective instabilities at the onset of convection in a porous medium with inclined temperature gradient and vertical throughflow. J Fluid Mech 641:475–487
5. Brevdo L, Ruderman MS (2009) On the convection in a porous medium with inclined temperature gradient and vertical throughflow. Part I. Normal modes. Transp Porous Media 80:137–151
6. Brevdo L, Ruderman MS (2009) On the convection in a porous medium with inclined temperature gradient and vertical throughflow. Part II. Absolute and convective instabilities, and spatially amplifying waves. Transp Porous Media 80:153–172
7. Delache A, Ouarzazi MN, Combarnous M (2007) Spatio-temporal stability analysis of mixed convection flows in porous media heated from below: comparison with experiments. Int. J. Heat Mass Transf 50:1485–1499
8. Diaz E, Brevdo L (2011) Absolute/convective instability dichotomy at the onset of convection in a porous layer with either horizontal or vertical solutal and inclined thermal gradients, and horizontal throughflow. J Fluid Mech 681:567–596
9. Dufour F, Néel MC (1998) Numerical study of instability in a horizontal porous channel with bottom heating and forced horizontal flow. Phys Fluids 10:2198–2207
10. Hirata SC, Ouarzazi MN (2010) Three-dimensional absolute and convective instabilities in mixed convection of a viscoelastic fluid through a porous medium. Phys Lett A 374:2661–2666
11. Joulin A, Ouarzazi MN (2000) Convection mixte d'un mélange binaire en milieu poreux. Comptes Rendus de l'Académie des Sciences – Series IIB – Mechanics-Physics-Astronomy 328:311–316
12. Prats M (1966) The effect of horizontal fluid flow on thermally induced convection currents in porous mediums. J Geophys Res 71:4835–4838
13. Rees DAS (1997) The effect of inertia on the onset of mixed convection in a porous layer heated from below. Int Commun Heat Mass Transf 24:277–283